HERON is jointly edited by:
STEVIN-LABORATORY of the department of Civil Engineering, Delft University of Technology, Delft, The Netherlands
and
INSTITUTE TNO for Building Materials and Building Structures. Rijswijk (ZH), The Netherlands.
HERON contains contributions based mainly on research work performed in these laboratories on strength of materials, structures and materials science.

Secretary:
G. J. van Alphen
Stevinweg 1
P.O. Box 5048
2600 GA Delft, The Netherlands
Tel. 0031-15-785919
Telex 38070 BITHD

HERON vol. 28 1983 no. 1

Contents

DYNAMIC ELASTO-PLASTIC MODEL FOR REINFORCED CONCRETE MEMBERS

C. van der Veen
Delft University of Technology
Stevinweg 1, P.O. Box 5048, 2600 GA Delft, The Netherlands

J. Blaauwendraad
Rijkswaterstaat, Structural Research, Utrecht
P.O. Box 20.000, 3502 LA Utrecht, The Netherlands

Publications in HERON since 1970

Preface

This report incorporates part of a graduation thesis submitted to the Delft University of Technology, the Netherlands. The object of the investigations carried out in the context of the graduation work in question was to ascertain whether combustible substances involving an explosion hazard should be permitted to be transported through underwater road tunnels. Attention was more particularly focused on the behaviour of the tunnel roof under explosion load conditions.

First, the load-resisting capacity of a reinforced concrete section under impulsive load was investigated, with particular reference to the effect of shear on the failure load. Next, a generally-applicable numerical beam model was developed with which a dynamic response in the *plastic* range can be simulated.

The graduation work as a whole was carried out within the Structural Mechanics division of the Department of Civil Engineering. An integrated subsidiary study was carried out in the Concrete Structural division under the direction of Professor Dr.-Ing. H. W. Reinhardt. The shear strength and rotational capacity of dynamically loaded beams were determined in this subsidiary study, which was undertaken with the advisory support of Dr. Ir. J. C. Walraven, to whom the authors wish to record their sincere thanks.

DYNAMIC ELASTO-PLASTIC MODEL FOR REINFORCED CONCRETE MEMBERS

Summary

It is becoming increasingly necessary to investigate the strength of reinforced concrete structures subjected to dynamic loading. Experience and knowledge relating to the non-linear dynamic behaviour of such structures is still limited, however. Attempts to solve this type of problems with the aid of a finite element approach soon encounter difficulties. An example of this consists in the correct representation of the appropriate collapse mechanism and more particularly in the problem of the numerical stability for the integration process required for solving the equations of motion with respect to time and made additionally awkward by the non-linear behaviour. These problems are associated with mathematical algorithms and are not relevant to the structural problem under investigation.

The authors anticipate considerable improvement in this sphere in the future, but at present they prefer an approximation which provides direct insight into the response of structures without involving too many difficulties with numerical problems. For this reason a simple well-tried beam model is applied. This discrete beam model consists of a number of indeformable segments (the elements) with hinges (the nodes) at their ends and joined to one another by means of flexural springs. The mass of each segment is conceived as concentrated in the hinges, as is also the dynamic load. The material properties are assumed to be elasto-plastic. The effect of loading rate on the material properties has also been taken into account. Two failure criteria are applied in the discrete mathematical model. Thus, in the elastic range ($M < M_p$) the concrete section is checked for strength, and in the plastic range the rotational capacity is not allowed to be exceeded. In other words, the shear strength (loadbearing capacity in shear) is calculated as a function of the moment-shear combination that occurs.

The treatment of the subject starts from formulae derived for static moment-shear combinations. It emerges that the (static) formula given by Rafla can be modified and suited to dynamically loaded structures ($M < M_p$). The effect of shear on the permissible rotational capacity can be expressed in a simple relation. Thus, the rotational capacity will have its maximum value if the shear force is zero; but the presence of shear force will reduce the rotational capacity.

The discrete model described here has been applied to analysing the elasto-plastic response of a beam subjected to an impulsive load. Two different examples are presented.

The first example is concerned with the response of a simply-supported beam under a uniformly distributed impulsive load. It appears that the distributions of the bending moments and shear forces are very different from those obtained for a comparable static load. Presupposing that no shear failure will occur (adequate shear reinforcement), plastic moments will be formed at some distance from mid-span. From here the plastic hinges will then move towards the middle of the span.

The second example considers a beam with fixed (fully restrained) ends. It approximately represents a strip of the roof of a road tunnel. The situation where a gas explo-

sion occurs in the tunnel is investigated. The distribution of the bending moments which is then produced bears a closer similarity to that associated with a static load, but the shear forces are still different, though less so than in the case of the simply-supported beam.

If no stirrups are provided, a shear failure criterion must be introduced. This will very greatly reduce the permissible explosion load, so that in most cases no plastic hinges will even be formed.

Conclusion

Analyses performed with the elasto-plastic discrete model show that this model is able to represent the response of a beam under impulsive load with sufficient accuracy. Though it is realized that the actual behaviour may be different in detail, the overall behaviour is correctly simulated. Available experimental results are in good agreement with the results derived from the model. This is certainly so with regard to the qualitative trend displayed, but the quantitative information obtained also shows fair agreement.

Dynamic elasto-plastic model for reinforced concrete members

1 Introduction

The possibility of analysing structures subjected to extreme dynamic loading is currently receiving a good deal of attention. The response to extremely high dynamic loads will be considered in this report. Such a load may occur, for example, in consequence of a (gas) explosion in a building or in a underwater tunnel. With regard to severe explosions, with a very low probability of occurrence during the service life of the (concrete) structure, a substantial amount of structural damage can be tolerated. The requirement that has to be fulfilled is that the structure must on no account suffer complete collapse. To cope with such loads it is necessary to rely on the plastic deformation capacity of a concrete structural section. In this context it is important to be able to predict the shear strength (loadbearing capacity in shear) of dynamically loaded structures, schematized as beams, under combinations of shear force and bending moment. This will be dealt with in Chapter 2.

Because the dynamic response is not confined to the elastic range of behaviour, a distinction has to be made as to the mode of shear failure. In the elastic range the *shear strength* of the concrete section has to be determined, while in the plastic range (where plastic hinges can form) the *rotational capacity* of a structural member is especially important. In order to predict the correct failure mechanism that will develop during the response, it is necessary to take account of the successive occurrence of various moment-shear combinations at one section of the schematized concrete beam. A direct consequence of the dynamic character of a load is the effect of the rate of loading upon the material properties of the structure. Under high loading rates the properties of both materials, i.e., concrete and reinforcing steel, will undergo changes. In relation to the shear strength of the concrete section the (dynamic) *tensile* strength of the concrete is certainly of importance. In order to determine the correct rotational capacity of a structural member it is necessary moreover to know the compressive ultimate strain of the concrete and the maximum elongation of the steel. These matters will be considered in Chapter 3.

Since plastic hinges may be formed during the response to dynamic loading, an analytical solution is not possible. Actually, the problem has become a physically non-linear time-dependent one. To obtain a solution it is necessary to apply a numerical method. Chapter 4 is concerned with this approach.

The beam could be schematized to a single-mass spring system, i.e., a system with one degree of freedom. In that approach the calculated shear force is of questionable accuracy, however. Yet it is an important quantity in determining the rotational capacity of a plastic hinge and in establishing an appropriate concrete section for combina-

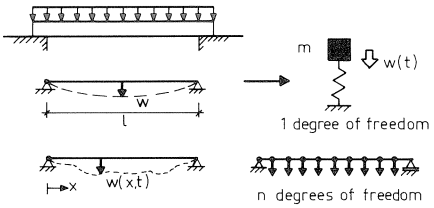

Fig. 1.1. Beam schematized to a single-mass spring system with one degree of freedom or to an n-mass spring system with n degrees of freedom.

tions of bending moment and shear force. In order to calculate the shear force correctly, as a function of position and time, it is necessary to employ a mathematical model possessing a sufficient number of degrees of freedom; see Fig. 1.1. The mathematical model developed for the purpose has been applied to two specific problems. These will be dealt with in Chapter 5.

2 Loadbearing capacity in shear

With reference to literature research some formulae for predicting the shear strength (loadbearing capacity in shear) under moment-shear (M-V) combinations will be presented. Because hardly any formulae for the prediction of the shear strength of *dynamically* loaded structures subjected to such combinations are to be found in the literature, the approach adopted here will start from formulae derived from static M-V combinations. By investigating the effect of various parameters used in formulae it can be indicated whether, on the one hand, the "static" formulae remain valid or whether, on the other hand, appropriately modified (higher or lower) values will have to be used.

In this treatment of the subject the following distinction is drawn as to the manner in which shear failure may occur:

1. shear *strength* $(M < M_{sy})$
2. rotational capacity $(M = M_{sy})$

In the first case the strength of a concrete section for combinations of a bending moment and a shear force has to be determined. So long as the yield moment M_{sy} has not yet been attained at a concrete section, the shear capacity of the section can thus be calculated. After the yield moment has been attained, the effect of the shear force on the deformation capacity of the concrete section must be ascertained. We therefore actually determine the permissible rotational capacity of a plastic hinge.

2.1 *Shear strength*

Slender beams *without* shear reinforcement will be considered here. The shear behaviour of rectangular beams depends to a considerable extent on the moment-shear (M/Vd) ration. In experiments in which the beam is loaded by a point load the ratio a/d is encountered in the literature, d being the effective depth and a the distance from the load to the support. These two ratios are comparable.

Depending on the magnitude of this ratio, a particular failure mechanisms occurs. The strength capacity can be calculated for each mechanism. For static loading cases the following classification into various types of failure mechanism is commonly adopted:

- bending moment failure (see rotational capacity);
- flexural shear failure (shear crack arising from flexural crack);
- tensile shear failure (diagonal crack in web);
- compressive shear failure (failure of compression diagonal);
- anchorage failure.

Because of the subdivision into "shear strength" and "rotational capacity" the "bending moment failure" mechanism is associated with the type "rotational capacity". The occurrence of *compressive* shear failure and anchorage failure is not considered here and is indeed not regarded as relevant with respect to rectangular non-prestressed beams.

The fact that only beams without shear reinforcement are considered does not constitute a restriction upon the general applicability of the formulae yet to be derived. The same formulae can be used if shear reinforcement *is* provided, because it is mostly assumed that V_c (with shear reinforcement) = V_c (without shear reinforcement). The overall transfer of force at a concrete section then comprises a superposition of V_c (shear force resisted by the concrete itself) and V_{sv} (shear force resisted by reinforcement). Hence:

$$V_u = V_c + V_{sv} \tag{1}$$

2.1.1 Flexural shear failure

If a shear crack develops from a flexural crack, the resulting failure is called flexural shear failure.

Investigation have shown that a great many variables have a distinct effect on the shear strength of structural members containing no shear reinforcement. They have also shown that many variables have virtually no effect on shear strength. The following are some important factors affecting the shear strength:

Tensile strength of the concrete

Both the *tensile* and the *compressive* strength of the concrete play an important part. Since the tensile strength is dependent on the compressive strength, however, empirical formulae often contain only the compressive strength.

Shear cracks are formed in consequence of the tensile strength being exceeded and determine the shear strength. Higher tensile strength is therefore associated with higher shear strength. The importance of the tensile strength is manifested in Kani's so-called comb model [2], in which the "teeth" between the cracks are conceived as cantilevers fixed at one end. Such a cantilever is subjected to loading in consequence of the bond of the longitudinal reinforcement and the interlock resistance across the cracks.

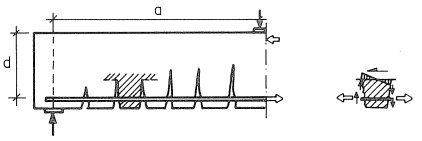

Fig. 2.1. Kani's comb model.

An inclined crack is formed when the tensile stresses at the fixed end of the cantilever become too large. The formation of an inclined crack is usually accompanied by failure; see Fig. 2.1.

Research by, among others, Taylor has shown the shear transfer at a flexurally cracked concrete section to comprise various components. He demonstrated that *in* the cracks a considerable transfer of shear stress occurs in consequence of the roughness of the crack faces (aggregate interlock) and dowel action of the longitudinal reinforcing bars, the respective shares of these two transfer components being estimated at 35–50% and 15–25% of the total shear capacity [3].

Percentage of tensile reinforcement
A higher reinforcement percentage increases the extensional stiffness of the "tie-rod", so that more flexural cracks will be formed, but the crack *width* will remain smaller (therefore greater aggregate interlock). The shear strength increases in consequence. So does the dowel action.

Depth of the member
The crack pattern and thus the shape and number of "concrete teeth" bounded by the cracks are affected by the depth of the beam. In deep beams the "teeth" are more constricted and more pronounced than in shallow ones, which results in a different (i.e., lower) shear strength (as asserted by Kani). A different explanation is given by Taylor and Swamy. They consider that larger crack widths are associated with an increase in scale, so that the contribution of aggregate interlock to the shear strength diminishes in importance. Greater depth of the beam therefore results in *lower* shear strength (= stress).

With the aid of fracture mechanics it has been shown by Reinhardt and Hillerborg that the size of the test specimen affects the rate at which the crack pattern develops and thus affects the shear strength. The larger the specimen, the lower the nominal shear strength ($= V/bd$). Thus the following relation [16] between the shear strength and the size (more particularly the depth) of the specimen was obtained: $\tau_u :: h^{-1/2}$. It is to be noted that, if sufficient shear reinforcement is present, there is hardly any decrease in shear strength with increasing beam depth.

Moment-shear ratio
If the load is applied close to the support, the formation of a shear crack will not necessarily result in failure, because in that case direct transfer of load to the support is

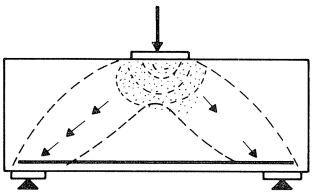

Fig. 2.2. Statically loaded beam with a multiaxial state of stress under the point load.

possible. This means that the shear strength increases with decreasing values of the ratio a/h. A second reason for the shear strength increase for $a/d < 2.5$ is bound up with the manner of load application to the beam. In virtually all static tests the load was applied in the form of a *point load.* A multiaxial state of stress develops under such a load, so that a high strength of the compressive zone is possible; see Fig. 2.2. When an inclined shear crack has formed, it will be arrested in the multiaxial stress zone. Further increase in the magnitude of the load is then even still possible. With uniformly distributed (dynamic) load such increase is unlikely. It is to be noted that, with reference to uniformly distributed load, the concept of shear slenderness ratio a/d is replaced by that of the ratio M/Vd.

For the reason stated above, Zsutty [8 and 9] gives two formulae for calculating the shear strength. The first formula (2) expresses the shear strength at the instant when inclined cracks are formed, while the second formula (3) expresses the shear strength at failure:

$$\tau_{cr} = 8.62 \sqrt[3]{f_c \varrho (Vd/M)}\, d^{1/4} \qquad M/Vd \geqslant 2.5 \tag{2}$$

$$\tau_u = 9.31 \sqrt[3]{f_c \varrho (Vd/M)}\, d^{1/4} \qquad M/Vd \geqslant 2.5 \tag{3}$$

where f_c denotes the cylinder (compressive) strength in N/mm^2, ϱ the reinforcement fraction, and d the effective depth of the beam in mm. (These two formulae have been converted to the dimensional units employed in this report).

For $M/Vd < 2.5$ both formulae have to be multiplied by $2.5\,Vd/M$. They then give a lower bound for which 75% of the observed values are higher. Only formula (2) is realistic because the increase in shear strength after the formation of cracks depends on, among other features, the crack pattern.

Statically indeterminate beams

Various investigators [10, 11, 12] have studied the question whether the shear behaviour of beams continuous over several supports is comparable with that of a simply-supported beam. The continuous beam considered in such investigations is usually a beam on three supports. From the moment diagram and shear diagram it follows that at the intermediate support a larger shear force V and also a larger bending moment M are acting than in the span. So it is not surprising that, certainly with high reinforcement

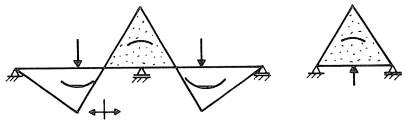

Fig. 2.3. With statically indeterminate beams the moment-shear ratio must be reckoned from the point of zero bending moment.

percentages, in most of the tests shear failure occurred at the intermediate support. This can be prevented by installing stirrups in the vicinity of that support.

When the shear strength was calculated in accordance with formulae (to be given below) derived from tests on simply-supported beams, there was found to be very good agreement.

General

The effect of the quantity of compressive reinforcement on the shear strength has not yet been established. Distribution of the longitudinal reinforcement - a large number of thinner bars as against a small number of thicker ones - has little effect on the shear stress. If the shear force is adopted as the criterion, a higher shear strength is attained for uniformly distributed load than for comparable loading by point loads. The reason is that in the flexurally cracked region, where the shear strength is relatively low, the shear force is also small in the case of uniformly distributed load.

2.1.2 Empirical formula

One of the best formulae for calculating shear strength has been given by Rafla [12]. Based on a statistical approach incorporating all the influencing parameters, it enables the average shear strength to be calculated from:

$$\tau_u = \alpha_u f_{cc}^{1/2} \varrho_s^{1/3} d^{-1/4} \qquad (\mathrm{N/mm^2}) \tag{4}$$

where f_{cc} is the cube (compressive) strength in $\mathrm{N/mm^2}$, while ϱ_s is in % and d in mm, and α_u is given by:

$$\begin{aligned} 1.0 \leqslant M/Vd \leqslant 2.0 \qquad & \alpha_u = 6.00 - 2.20(M/Vd) \\ 2.0 \leqslant M/Vd \leqslant 3.5 \qquad & \alpha_u = 0.795 + 0.293(3.5 - M/Vd)^{2.5} \\ M/Vd \geqslant 3.5 \qquad & \alpha_u = 0.90 - 0.03 M/Vd \end{aligned}$$

The formula was verified against 422 test results, and the main parameters were investigated within the following limits:

concrete grade	f_{cc}	$= 7.5\ \mathrm{N/mm^2}$–$88\ \mathrm{N/mm^2}$
reinforcement percentage	ϱ_s	$= 0.5\%$–7.5%
depth of beam	h	$= 70\ \mathrm{mm}$–$1200\ \mathrm{mm}$
shear slenderness ratio	a/d	$= 1.0$–10.0
width/depth	b/h	$= 0.15$–5.8
yield point of steel	f_{sy}	$= 210\ \mathrm{N/mm^2}$–$900\ \mathrm{N/mm^2}$

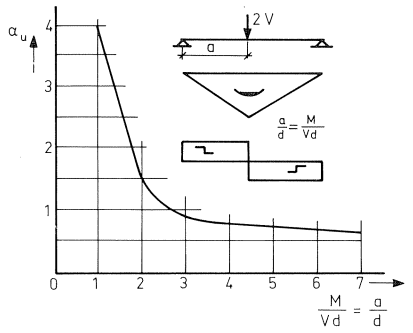

Fig. 2.4. The value α_u as a function of the shear slenderness ratio $a/d = M/Vd$.

By multiplication of formula (4) by 0.83 a 5% lower limit for the shear strength is obtained.

2.1.3 Tensile shear failure

In this mode of shear failure no cracks arising from flexural cracking on the underside of the beam are formed. The first inclined cracks are observed in the web of the beam, these being formed when the principal tensile strength is attained. If sufficient shear reinforcement is available, equilibrium will be restored. But if the beam contains no (or insufficient) shear reinforcement, it will not be possible for a fresh state of equilibrium to establish itself: the crack will therefore extend further and the beam will fail.

We shall now start from a concrete section loaded mainly in shear and shall adopt as the criterion for this loading:

$$M/Vd \leqslant 1$$

From the equilibrium of stresses at the neutral axis it follows that the tensile strength f_{ct} is equal to τ; see Fig. 2.5. Assuming a parabolic shear stress distribution over the depth of the beam, we obtain for the nominal shear strength:

$$\tau_u = 0.67\tau, \quad \text{with} \quad \tau = f_{ct} \qquad (\text{N/mm}^2) \tag{5}$$

The transfer of shear force is expressed by:

$$V_u = bh0.67f_{ct} \qquad (\text{N}) \tag{5a}$$

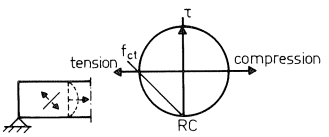

Fig. 2.5. From the equilibrium of stresses at the neutral axis it follows that the tensile strength f_{ct} is equal to τ.

In further treatment of the problem the characteristic value will be substituted for the tensile strength. The characteristic short-term tensile strength f_{ctk} is calculated as follows:

$$f_{ctk} = 0.87(1 + 0.05 f_{cc}) \qquad (\mathrm{N/mm^2})$$

Since Rafla's formula is valid only for $M/Vd > 1$, the following value:

$$\tau_u = 0.67 f_{ctk} \tag{6}$$

constitutes the upper limit for small moment-shear ratios.

2.1.3.1 Direct shear

Direct shear may occur in a completely cracked concrete section, the shearing planes being parallel to the force. A cracked section may occur in floor structures, beams, etc. as a result of defective workmanship in constructing them. Transfer of force in the event of parallel displacement of the two crack faces in opposite directions is effected at the contact surfaces between the aggregate particles on one side of the crack and the matrix material on the other side (aggregate interlock); see Fig. 2.6.

The maximum shear strength is attained at the instant when yielding occurs in the reinforcement that crosses the crack. Now the gripping force cannot undergo further increase and the contact faces will move apart, so that the contact area decreases and the resistance diminishes. The lower limiting value usually adopted [16] for this shear strength is:

$$\tau_u = 1.4 + 0.8 \varrho f_{sy} \qquad (\mathrm{N/mm^2}) \tag{7}$$

$$\tau_u \leqslant 0.3 f_c \qquad (f_c = \text{cylinder strength})$$

A drawback of the formula for τ_u is that, for the values of ϱf_{sy} employed in practice, the strength of the concrete has no effect.

Walraven [15] has given the following relation, in which the concrete strength does occur, to express the shear strength:

$$\tau_u = c_1 (\varrho f_{sy})^{c_2} \qquad (\mathrm{N/mm^2}) \tag{8}$$

where $c_1 = f_{cc}^{0.36}$ and $c_2 = 0.09 f_{cc}^{0.46}$.

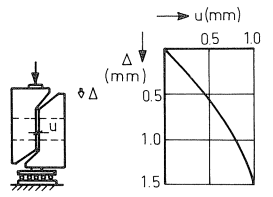

Fig. 2.6. Test set-up for determining the aggregate interlock associated with a particular crack width.

A 5% lower limit is given by:

$$\tau_u = 0.85 c_1 (\varrho f_{sy})^{c_2} \qquad (\mathrm{N/mm^2}) \tag{9}$$

In general, formula (7) or (9) is not employed in calculations relating to beams, because the depth of cover to the reinforcement is too small to prevent the concrete spalling away from the reinforcement. All the same, in Chapter 5 formula (7) will be applied to a beam section, but in that case the location of the reinforcement has been suitably adapted!

2.1.4 Dynamic influences

As yet (too) little is known about moment-shear combinations in dynamically loaded structural members. For this reason, data obtained from investigations on statically loaded and statically determinate beams will provide the starting point of this treatment of the problem. Consider a 5% lower limit for Rafla's formula:

$$\tau_u = 0.83 \alpha_u f_{cc}^{1/2} \varrho_s^{1/3} d^{-1/4} \qquad (\mathrm{N/mm^2}) \tag{10}$$

We shall now find out what parameters change under the influence of dynamic loading. Such loading gives rise to rates of strain or deformation ($\dot{\varepsilon}$) in the structure. Research [18] has shown that the *compressive* strength of the concrete changes as a function of the strain rate. The tensile strength of the concrete is not directly incorporated in formula (10). Instead, the cube strength $f_{cc}^{1/2}$ has been introduced as the governing quantity for the concrete grade (i.e., the quality of the concrete in terms of strength). Although there exists a statistically based empirical relationship between the tensile and the compressive strength of concrete, this relationship changes for different strain rates [19]. For this reason the factor $f_{cc}^{1/2}$ in formula (10) is left unchanged, but a direct relationship between the shear strength τ_u and the tensile strength of the concrete is established.

Consider a concrete section which has cracked in bending. According to Taylor, the various components involved in shear transfer in beams without shear reinforcement make the following proportional contributions to such transfer:

V (compressive zone) = 20–40%
V (aggregate interlock) = 35–50%
V (dowel action) = 15–25%

We shall investigate what relation there exists between the tensile strength of the concrete and the above-mentioned components. The strength (loadbearing capacity) of Kani's comb model is linearly dependent on the tensile strength of the concrete. Hence it follows that the shear component of the compressive zone is likewise linearly dependent on the tensile strength. Formulae for calculating the dowel action capacity of a layer of reinforcing bars are given in [20]. The starting point for these formulae is provided by the differential equation of the elastically supported beam (the reinforcing bar). Up to the occurrence of the first crack the following relation holds for the dowel force:

$$V(\text{dowel}) = f_{ct}\, b_n\, l_z$$

where:

f_{ct} = tensile strength of the concrete
$b_n = b - \Sigma \Phi_d$ = net width of the concrete
Φ_d = diameter of a reinforcing bar
l_z = characteristic length for distribution of vertical tensile strength

The length l_z is affected mainly by the number of reinforcing bars and to a less extent by the strength of the concrete. V (compressive zone) is linearly dependent on the tensile strength of the concrete, and V (dowel) is also - approximately - *linearly* dependent on the tensile strength of the concrete. We shall now assume that under dynamic loading conditions the shear component V (aggregate interlock) remains constant and transfers 50% of the total static shear force. This means that formula (10) must be multiplied by $\frac{1}{2}(f_{ctd} + f_{ctk})/f_{ctk}$ for calculating the dynamic shear strength, where f_{ctd} is the dynamic tensile strength of the concrete.

The loading rate has no effect on the factor $\varrho_s^{1/3}$ in formula (10). This factor expresses the influence of the extensional stiffness $E_s A_s$ of the "tie rod". Under dynamic loading, however, E_s remains *constant* up to the yield point [34], neglecting the part played by the concrete in the tensile zone (tension stiffening).

Now let us consider the factor α_u which is dependent on the moment-shear combination M/Vd that occurs. In Section 2.2.1 it is stated that under uniformly distributed (dynamic) load, for low values of the M/Vd ratio, a marked increase in shear strength will take place more slowly. There is, however, a second reason why this marked increase will lag behind or will occur only for smaller values of M/Vd.

In the first place it must be taken into account that the "dynamic" deflection curve differs from the static deflection curve. Hence it follows that the bending moment and shear diagrams under dynamic conditions may differ from those under static conditions. In the static case there occurs an increase in shear strength already for $M/Vd < 3.5$. Rafla's formula is based on data obtained from structures under static load, so that this low M/Vd ratio always occurs directly beside a support. In consequence, part of the load can be transferred by direct transmission, via a thrust arch, to the support; see Fig. 2.2. In dynamically loaded beams, however, such low values of M/Vd may occur also at sections in the mid-span region, in which case no such direct transfer of load to the support can take place. Therefore Rafla's formula is not necessarily correct for every section of the dynamically loaded beam. For this reason we shall adjust the factor α_u and calculate it also for $M/Vd < 3.5$ from $\alpha_u = 0.9\text{–}0.03 M/Vd$, so that a marked increase now rightly lags behind. However, Rafla's formula is valid only for $M/Vd > 1$. For lower values of this ratio tensile shear failure occurs under dynamic load; see Section 2.1.3.

Tensile shear failure

From the static relation $\tau_u = 0.67 f_{ctk}$ it follows that the shear strength is linearly dependent on the tensile strength, so that the dynamic shear strength can be calculated from the following formula:

$$\tau_{ud} = \frac{f_{ctd}}{f_{ctk}} 0.67 f_{ctk} = 0.67 f_{ctd} \tag{12}$$

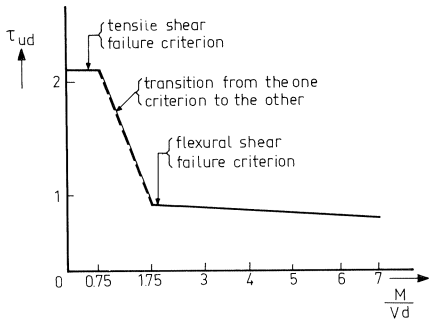

Fig. 2.7. The adopted dynamic shear strength τ_u as a function of M/Vd.

We now have an expression for the shear strength for $M/Vd < 1$ (tensile shear failure) and also for $M/Vd > 1$ (Rafla, adapted). It is to be expected that, for a certain moment-shear ratio, there will exist a transition zone between the two failure mechanisms. Therefore a straight line has arbitrarily been drawn from the shear strength associated with $M/Vd = 0.75$ to the shear strength associated with $M/Vd = 1.75$; see Fig. 2.7. The value $M/Vd = 0.75$ has been chosen as the lower limit of $M/Vd < 1$, while $M/Vd = 1.75$ is situated intermediately between $M/Vd = 1$ and $M/Vd = 3.5$. This last-mentioned arbitrarily chosen M/Vd ratio takes account of the circumstance that increase in shear strength will occur only for a lower value of M/Vd (no point load and support!).

Summary of relationships for dynamic shear strength/shear force:

$M/Vd < 0.75$

$$\tau_{ud} = 0.67 f_{ctd} \tag{12}$$

shear force

$$V_{cd} = 0.67 f_{ctd} bh \tag{12a}$$

$M/Vd > 1.75$

$$\tau_{ud} = \alpha_d f_{cc}^{1/2} \varrho_s^{1/3} d^{-1/4} \frac{(f_{ctd} + f_{ctk})}{2 f_{ctk}} 0.83 \tag{11}$$

where

$$\alpha_d = (0.9 - 0.03 M/Vd)$$

shear force

$$V_{cd} = \alpha_d V_n \tag{11a}$$

where

$$V_n = f_{cc}^{1/2} \varrho_s^{1/3} d^{3/4} b \frac{(f_{ctd} + f_{ctk})}{2 f_{ctk}} 0.83$$

Note: If the factor α_d for $M/Vd < 0.75$ is equal to $\alpha_d = V_{cd}/V_n$, then the shear force $V_{cd} = \alpha_d V_n = (V_{cd}/V_n)V_n = V_{cd}$. The advantage of this is that in a computer calculation the shear force can be calculated by any M/Vd ratio via $V_{cd} = \alpha_d V_n$ (V_n = constant!).

2.2 *Rotational capacity*

Various investigators [23–29] have studied the phenomenon of the largest possible plastic rotation of a small portion of a beam under a combination of bending moment and shear force. The wide scatter displayed by the test results is notable. First, some relevant concepts will be considered more closely, with reference to a beam loaded as shown in Fig. 2.8.

If the yield moment M_{sy} is attained at a concrete section, further load increase will be attended by plastic deformation occurring over a certain length of the beam, called the plastic length l_p. A (plastic) hinge is conceived to occur at the section where the extreme bending moment is produced. Cracked as well as uncracked sections will be present within the plastic length. As implied by the development of the plastic length, it is really no longer correctly possible to describe the behaviour of the beam in terms of specific sections. Instead, the average behaviour of a certain *portion* of the beam is usually considered. This behaviour is represented in a moment-rotation (M-Φ) diagram, the rotation Φ being equal to the summation of curvatures over a certain length of the beam Δl, $\Phi = \int \varkappa \, ds$. If the curvatures over a beam portion of length Δl are equal and constant, then $\Phi = \varkappa \Delta l$. In that case the M-Φ diagram is similar in shape to the M-$\varkappa$ diagram; see Fig. 2.9.

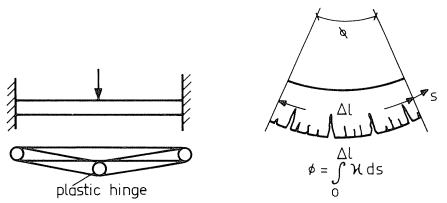

Fig. 2.8.

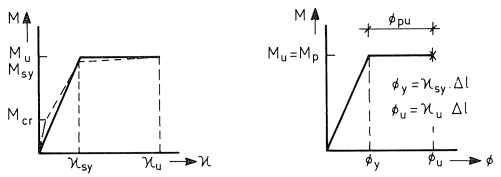

Fig. 2.9. Left, the schematized two-branched moment-curvature diagram; right, the two-branched moment-angle diagram for a beam portion of length Δl.

So it is possible to proceed from the section behaviour (M-$\varkappa$) to the behaviour of a small beam portion of length Δl (M-Φ relation). Since, if shear force is present, the permissible plastic rotation Φ_{pV} is of particular interest, Δl is replaced by the plastic length l_p.

We can now schematize the three-branched M-$\varkappa$ diagram to a two-branched diagram, as in Fig. 2.9. For this purpose the plastic moment M_p in the two-branched diagram is equated to the failure moment M_u in the three-branched diagram. The curvature $\varkappa_{sy}$ is the curvature at which the main reinforcement has attained the yield strain or the 0.2% proof stress.

How are we to conceive qualitatively the effect of the shear force upon the rotational capacity? In the plastic range of behaviour it is assumed that the proportion of shear transfer by aggregate interlock at the cracks is negligible (because then the cracks are very wide), so that shear is transferred by the concrete compressive zone only. However, when the yield moment M_{sy} has been attained, the compressive zone will become steadily smaller as deformation increases. When rotation occurs, the concrete compressive zone is loaded by a virtually constant normal force N_c and a shear force V. At a particular magnitude of the deformation the compressive zone becomes so small that failure occurs. If no shear force is acting on the section, greater deformation of the section is possible. The shear force therefore *reduces* the deformation capacity (rotational capacity) of the concrete section.

On the basis of research some formulae for calculating the rotational capacity of a beam portion under the influence of bending moment and shear force are given in [29]. The depth h of the beam has been adopted as characterizing the plastic length l_p. For a beam fixed (restrained) at its ends the plastic length at a fixed end is equal to h and in the span it is equal to $2h$. The following formula for calculating the rotational capacity is given:

$$\Phi_{pV} = (1 - 2r)\Phi_{pu} \tag{13}$$

where:

r $= (V - V_{sv})/V_c$; if $V_{sv} > V$, then $r = 0$
V_c $= bh\tau$ (VB 1974), with τ (VB 1974) $= 0.5 f_{ct}$*
V_{sv} $\simeq 0.9 \varrho_{sv} f_{sy} bh$
$\Phi_{pu} = (\varkappa_u - \varkappa_{sy}) l_p$, where $l_p = h$
Φ_{pV} = permissible plastic rotation

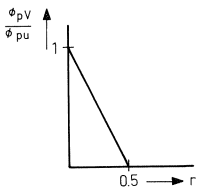

Fig. 2.10. The relative rotational capacity as a function of the parameter r. The value of r is determined at the instant when the yield moment is attained.

* VB 1974 = Netherlands Code of Practice for Concrete, 1974 version.

The product $h(\varkappa_u - \varkappa_{sy})$ is conceived as the largest possible value Φ_{pu} for the rotational capacity which occurs if $V = V_{sv}$ (i.e., if all the shear force is resisted by shear reinforcement). The calculation of the failure moment (ultimate moment) $M_u (= M_p)$ is normally based on a concrete compressive strain $\varepsilon_{cu} = 0.35\%$. Substantially larger values of this strain have been found in the experiments, however, this being due more particularly to the presence of compressive stresses in the compressive zone which were due to bearing reactions and which acted in the vertical direction. In such cases it is permissible, but only for the calculation of $\varkappa_u$, to adopt a value of 0.7% for ε_{cu}. It must then be checked that the magnitude of the steel elongation before reduction of area ε_{stu} is adequate.

2.2.1 Rotational capacity in dynamically loaded structures

In considering the transfer of shear force in a dynamically loaded structure there is no reason to suppose that such transfer will take place in a different manner from that in a statically loaded structure as already described. However, in order to be able to apply them to dynamic loading conditions, we must take a closer look at some of the parameters involved. More particularly, two parameters deserve attention, namely, the shear transfer by the concrete compressive zone alone (V_c) and the maximum plastic rotation (Φ_{pu}).

V_c The properties of concrete undergo some change under dynamic loading. With an increase in loading rate both the concrete *tensile* and the concrete compressive strength can be expected to increase. It is therefore reasonable to suppose that the biaxial concrete stress* [31] which governs the failure of the compressive zone will have a somewhat higher value than in the case of comparable static loading. Hence: for a given depth x of the compressive zone, V_c (dynamic) is greater than V_c (static).

Φ_{pu} The maximum plastic rotation is equal to $\Phi_u - \Phi_y$, while the maximum rotation Φ_u is introduced as the product of the (theoretical) curvature at failure $\varkappa_u$ and the plastic length $l_p (= h)$ $\Phi_u = \varkappa_u l_p = \varkappa_u h$.

Many influencing factors are comprised in l_p. These will here be considered only in qualitative terms. The plastic length in which the reinforcing steel yields or undergoes plastic strain depends upon, among other factors, the reinforcement percentage and the bending moment distribution in the number.

Reinforcement percentage

A sufficiently high percentage of reinforcing steel is necessary in order to obtain good distribution of cracking over the length l_p.

* It is now considered that crack propagation (fracture mechanics) is the governing factor with regard to failure.

Distribution of bending moment

If the bending moment diagram displays a peak, cracking can spread only over a small region of the member. In consequence, cracking will be concentrated at one wide crack. A direct disadvantage of this situation is that the elongation before reduction of area of the steel will have to be large, because the deformation capacity will have to be provided by the relatively short length of reinforcing bar where slip between the bar and the surrounding concrete occurs. Since the possibility of a peaked moment diagram cannot be ruled out in dynamically loaded structures, it is necessary to use steels possessing large elongation before reduction of area. Furthermore, it must be taken into account that in dynamically loaded structures plastic hinges may develop at different sections of the members from those in statically loaded structures. Partly on account of the possible occurrence of a peaked moment diagram, we propose - in order to be on the safe side - to take the plastic length as equal to h for each hinge. This differs from the assumption made for the statically loaded beam, for which the plastic length is $l_p = h$ ($\varepsilon_{cu} = 0.7\%$) at the fixed end and $l_p = 2h$ ($\varepsilon_{cu} = 0.35\%$) in the span.

The compressive strain of the concrete will decrease with increasing rate of loading, so that the plastic rotation will also be less than in statically loaded structures.

We define again $\Phi_u = \varkappa_u l_p$, where $l_p = h$, and propose adopting the following relation between the permissible plastic rotation Φ_{pV} and the parameter r:

$$\Phi_{pV} = (1 - r)^2 \Phi_{pu} \qquad \text{see Fig. 2.11} \tag{14}$$

where:

r $= (V - V_{sv})/V_{cd}$ determined at the instant when the yield moment is attained; $r = 0$ if $V < V_{sv}$

$\Phi_{pu} = (\varkappa_u - \varkappa_{sy})h$

V_{cd} $= \tau_{ud} bh$, see formula (11a)

It appears from the above relation that for $r > 0.5$ a certain, though small, amount of rotation is still considered permissible, as contrasted with the relation of the static case. Closer examination of the test results reported in [29] shows that for statically loaded structures, too, some rotation is still possible for $r > 0.5$. Presumably in order to keep the static formula as simple as possible the CUR-VB Committee [29] adopted a linear relation between Φ_{pV} and r.

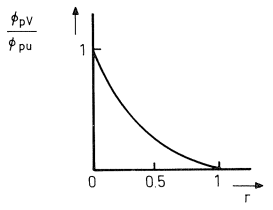

Fig. 2.11. The (relative) plastic rotation as a function of the parameter r.

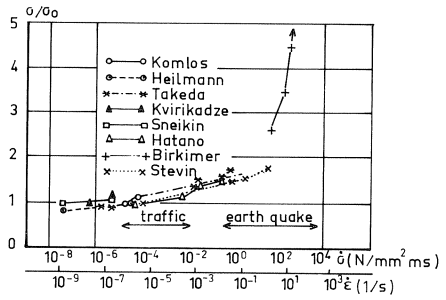

Fig. 3.1. Tensile strength as a function of the rate of strain $\dot{\varepsilon}$ (from [17]).

3 Material properties

As will have become apparent from the preceding chapter, the tensile strength of the concrete is one of the most important parameters in calculating the shear strength. The quantitative effect that the loading rate, which determines the rate of strain at the concrete section, has upon the tensile strength has to be established. However, he compressive strength and the modulus of elasticity will also change under high rates of strain. So in order to obtain a σ-ε diagram which may be used in dynamically loaded structures it will be necessary to scrutinize the literature to find out what effect the loading rate has upon the properties of concrete in general.

3.1 *Tensile strength of concrete*

The direct tensile strength of concrete as a function of the loading rate is reviewed in [17]; see Fig. 3.1. It appears that the average tensile strength f_{ctd} (N/mm^2) can suitably be plotted as a function of the stressing rate $\dot{\sigma}$ (N/mm^{2}ms).

$$\ln f_{ctd} = 1.51 + 0.042 \ln \dot{\sigma} \qquad ([18], \text{page } 105) \tag{15}$$

The static characteristic tensile strength can be calculated from:

$$f_{ctk} = 0.87(1 + \tfrac{1}{20} f_{cc}) \tag{16}$$

3.2. *Compressive strength and strain of concrete*

Experimental research has shown that the ultimate strength of concrete increases and

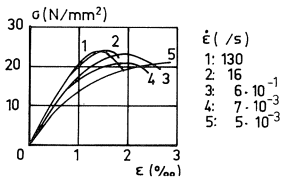

Fig. 3.2. Stress-strain relation for various rates of strain (Hjorth).

the ultimate strain decreases at high rates of loading. Although various investigators give relations expressing the compressive strength of concrete under high loading rates. we consider Hjorth's method [32] to be preferable for the present purpose. It enables both the compressive strain and compressive strength of concrete to be calculated. Hjorth tries to explain the time-dependent short-term behaviour, such as for example the increase in ultimate strength and the decrease in ultimate strain, by basing himself on the time-dependent long-term behaviour, such as for example creep or relaxation. The formulae for ε_{cu} obtained in this way are, however, implicit expressions and therefore have to be solved by an iterative procedure. This is rather time-consuming. The σ-ε relation for a number of different strain rates is given in graph form in [17]; see Fig. 3.2.

3.2.1 Modulus of elasticity

Kvirikadze [35] gives the relation between the actual modulus of elasticity. E_c and the stress increase with time:

$$E_{cd} = 0.1 E_c \left(\log \frac{\dot{\sigma}}{\dot{\sigma}_0} + 10 \right) \qquad (\mathrm{N/mm^2}) \tag{17}$$

where $\dot{\sigma}_0 = 0.5\ \mathrm{N/mm^2/s}$ is the stress increase rate in a static test. It is to be noted that a comparable relation is given for the compressive or the tensile strength of the concrete:

$$f_{cd} = 0.1 f_c \left(\log \frac{\dot{\sigma}}{\dot{\sigma}_0} + 10 \right) \qquad (\mathrm{N/mm^2}) \tag{18}$$

3.3 *Reinforcing steel*

Hjorth tested some types of reinforcing steel and determined the relation between the ultimate strength, the yield point and the ultimate strain, on the one hand, and the loading rate, on the other. The results show that:

- the yield stress increases more than the ultimate strength;
- the ultimate strain is almost constant, except in the non-heat-treated steels: for these the ultimate strain decreased.

This last-mentioned result is at variance with the experimental data obtained by Ammann et al. [36]. These investigators come to the conclusion that the elongation before reduction of area, measured on attainment of the tensile strength, *increases*. For cold-worked reinforcing steel this increase may be as much as 180%, whereas an increase of 30% was measured for hot-rolled reinforcing steel ($\dot{\varepsilon} = 5\ \mathrm{s}^{-1}$). The largest elongation before reduction of area occurs, as an absolute value, always in hot-rolled reinforcing steel when strain rates of op to $\dot{\varepsilon} = 5\ \mathrm{s}^{-1}$ are applied. Therefore in this report preference is given to using hot-rolled steel, for which the elongation before reduction of area under dynamic conditions has been taken as equal to the static elongation of *10%*.

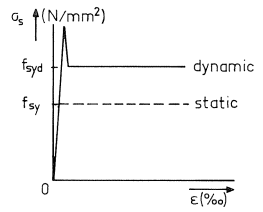

Fig. 3.3. Schematized dynamic σ-ε diagram showing an upper and a lower yield point.

Characteristic of the behaviour of steels subjected to high loading rates is the brief presence of a high upper yield point, directly followed by a lower yield point; see Fig. 3.3. Mainstone [34] shows that according as the static strength of reinforcing steel is higher the increase associated with rapid loading is less. It further appears that the E_s modulus is not affected by the loading rate!

At the conference on "Material properties at high strain rates" (Oxford, 1979) a formula was presented which establishes the relation between the (lower) yield point and the strain rate. Known as the Cowper Symonds relation, this formula is as follows:

$$\frac{\sigma_{syd}}{\sigma_{sy}} = 1 + \left(\frac{\dot{\varepsilon}_s}{40}\right)^{1/5} \tag{19}$$

and is valid in the range $10^{-7} < \dot{\varepsilon}_s < 10^6$.

At that conference the warning was moreover uttered that material properties determined under laboratory conditions of testing cannot be directly applied to the material in an actual structure. In a structure inertial forces will occur. Hence the higher values for the material properties are obtainable only with a *limited* degree of accuracy. This latter statement applies of course not only to steel, but also to concrete.

3.4 *Average dynamic material properties*

As indicated in the preceding section of this report, sufficient accuracy is obtained when average dynamic material properties are introduced into the calculations. This will be illustrated with the aid of an example.

3.4.1 Stress-strain diagram for reinforcement (grade FeB 400)

Suppose that a yield moment occurs at a concrete section at a time *between 0.01 s and 0.1 s,* i.e., after 0.05 s on average. The enhancement factor for the reinforcing steel, according to formula (19), will then be:

$$\frac{\sigma_{syd}}{\sigma_{sy}} = 1 + \left(\frac{0.04}{40}\right)^{1/5} = 1.25$$

where:

$$\dot{\varepsilon}_s \simeq \frac{2.0 \times 10^{-3}}{0.05} = 0.04 \text{ s}^{-1}$$

If the steel employed is of grade FeB 400, its yield point will be $1.25 \times 400 = 500$ N/mm^2. According VB 1974 the design value for the compressive strength must not exceed 420 N/mm^2. This requirement applies both to static and to dynamic loading. The ultimate strain (ε_{su}) for hot-rolled reinforcing steel is taken as equal to the static ultimate strain, which is 10%. The stress-strain diagram is presented in Fig. 3.4.

3.4.2 Stress-strain diagram for concrete in compression (concrete grade B 22.5)

Suppose that the yield moment in a structure must be attained within 0.1 s. For an average of approximately 0.05 s the stress increase rate is $\dot{\sigma} \approx 450$ N/mm^2/s. Substituted into formula (17) thos gives the following relation:

$$E_{cd} \approx 1.3 E_c$$

For grade B 22.5 this means:

$$E_{cd} \approx 1.3 \times 28000 = 36400 \text{ N/mm}^2$$

For calculating the compressive strain of the concrete we shall make use of Fig. 3.2 (Hjorth). Now the strain rate $\dot{\varepsilon}$ must be known. It is approximately 0.04 1/s or 4% per second. From Fig. 3.2 No. 3 ($\dot{\varepsilon} = 0.6$ 1/s) it appears that $\varepsilon_{cu} = 0.175$–0.18%. We shall adopt a lower limit $\varepsilon_{cu} = 0.175$% for the compressive strain of the concrete and bear in mind that this value is applicable also if the yield moment in a structure is attained within 0.01 s!

Formula (18) results in an enhancement factor of 1.3 for the compressive strength of the concrete as well. For grade B 22.5 the cylinder (compressive) strength is 18 N/mm^2, so that then $f_{cd} = 1.3 \times 18 = 23.4$ N/mm^2. According to VB 1974 the dynamic compressive strength must not exceed the characteristic cube (compressive) strength. This condition imposes an upper limit of $f_{cd} = 22.5$ N/mm^2 for the compressive strength of the concrete.

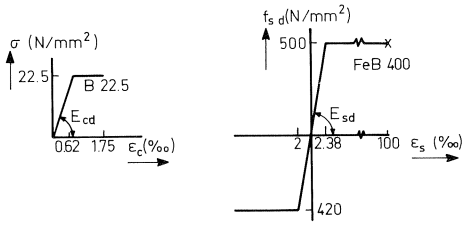

Fig. 3.4. Stress-strain relation for concrete (B 22.5) and reinforcing steel (FeB 400). The condition to be satisfied is that the yield moment in a structure must be attained within 0.1 s.

Moment-curvature diagram

The stress-strain diagrams (dynamic) obtained for concrete and for steel are shown in Fig. 3.4. With the aid of these diagrams we can calculate the moment-curvature diagram for dynamically loaded concrete sections. Multiplication of the curvature by the plastic length $l_p = h$ gives the moment-rotation diagram, which is similar in shape to the moment-curvature diagram.

For calculating the ultimate moment M_u we shall neglect the compressive reinforcement (if any) present in the concrete section. However, for calculating the curvature, any compressive reinforcement will have to be taken into account. For the ultimate curvature $\varkappa_u$ we must adopt the lower of the following values:

$$\varkappa_u = \varepsilon_{cu}/x \qquad \text{(concrete is the governing material)}$$
$$\varkappa_u = \varepsilon_{su}/(d-x) \qquad \text{(steel is the governing material)}$$

where:

x = depth of compressive zone of concrete
$\varepsilon_{su} = 10\%$ (hot-rolled reinforcing steel)

3.4.3 Hysteresis

Reinforced concrete is schematized to a two-branched moment-curvature diagram with elasto-plastic behaviour. Plastic hinges may occur in a dynamically loaded beam. After the tensile reinforcement at a concrete section has undergone yielding over a certain length, the phenomenon of "alternating yield" may occur. For a proper description of this phenomenon it is necessary to consider hysteresis behaviour.

The literature has been perused [37, 42] with a view to finding out what models are available for representing hysteresis. The general trend exhibited by such models is that the stiffness decreases with each circuit of the hysteresis curve. But all these models are applicable to loading cases where an *alternating* dynamic load remains acting for some time (seconds), e.g., in an earthquake. In our case we only wish to describe the response of a dynamic load which acts for a short time, e.g., a pulse-type or explosion load. This justifies the expectation that, after the load has been applied to the structure, the hysteresis curve is passed through only once, because of the strong plastic damping effect, so that the structure fades out in the "elastic" branch. For this reason the idealized hysteresis diagram, as shown on the right in Fig. 3.5, is permissible.

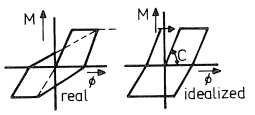

Fig. 3.5. On the left is shown an example of a hysteresis curve which may be adopted for an alternating load of long duration (earthquake); the schematized curve adopted in the present treatment of the subject is shown on the right.

4 Mathematical model

In the foregoing chapters it has been established what shear strength a dynamically loaded beam can develop. We are now able to ascertain the strength of a concrete section subjected to a combination of bending moment and shear force. Also, the effect of shear upon the rotational capacity of a plastic hinge can be determined.

Hence it follows that the dynamic load may of such magnitude that it becomes necessary to utilize the plastic deformation capacity of the concrete section in order to be able to resist such a load. In this way a physically non-linear time-dependent problem arises. It is not yet possible to provide an analytical solution for this non-linear problem, and for this reason a numerical method has to be employed in order to arrive at a solution.

The beam could be schematized to a single-mass spring system, i.e., a system with one degree of freedom. That would, however, presuppose that the lowest natural vibration mode is representative of the (elastic) response analysis. The lowest natural vibration mode is approximately similar to the elastic deflection curve of the beam subjected to gravity loading. This assumption implies that the moment and shear distribution in the dynamically loaded beam is *similar* in shape to the distribution of force which occurs in a beam under static load (see Fig. 4.1.). However, this will certainly not be the case if dynamic pulse-like loads are acting. This means that in a system possessing one degree of freedom more particularly the calculated shear force will be questionable. Yet this shear force is an important quantity for determining the rotational capacity of a plastic hinge and for assessing the strength of a section with regard to combinations of a bending moment and shear force. Now in order to calculate the shear force correctly, as a function of position and time, it is necessary to employ a mathematical model possessing a sufficient number of mass degrees of freedom. From the what has been said above it emerges that the numerical model should fulfil the following requirements:

- describe the physical non-linear behaviour and hysteresis;
- have a sufficient number of mass degrees of freedom.

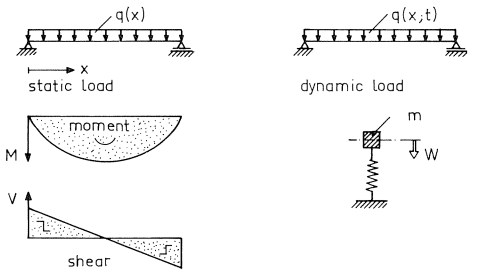

Fig. 4.1. A single-mass spring system produces a dynamic distribution of forces which is similar to that of a beam under static load.

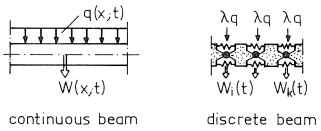

Fig. 4.2. Comparison between a physically continuous and a discrete beam model.

4.1 *Description of the mathematical model*

The point of departure is a beam which, on being loaded perpendicularly to its axis, undergoes only a deformation due to bending in the plane of loading. The physically continuous beam is now replaced by a discrete model; see Fig. 4.2.

A discrete (beam) model such as has been described by, among others, Blaauwendraad [43] has been chosen. Although this beam model as presented in [43] is applicable to statically loaded beams, the same theory can also suitable be used for dynamically loaded beams. In this latter case the inertial loading is also taken into account.

The discrete model comprises a number of indeformable segments (the elements) of length λ joined together by hinges (the nodes) and rotation springs, while the mass m of each segment is concentrated in the hinges. The uniformly distributed load $q = q(x; t)$ is replaced by an equivalent set of point loads acting at the hinges. For a constant segment length λ the magnitude of the point load at each hinge is λq. The physically non-linear material behaviour can be simulated by giving the springs interconnecting the segments an elasto-plastic spring characteristic. The dynamic load $q(x; t)$ is given as a function of time or, in a more general way, of position and time. The response of the structure (w, a, V, M, etc.) is also a function of position and time. The following partial differential equation holds for the continuous model:

$$EIw_{,xxxx} = q(x; t) - f(x; t) \tag{20}$$

where $f(x; t) = \mu w_{,tt}$ (inertial load)

This differential equation is valid only in the elastic range. Formula (20) is identical with the loading case of a statically loaded beam on which the uniformly distributed load is equal to $q(x) - f(x)$. The left-hand term in this formula is actually the elastic (spring) force which, in the final discrete model, is equal to $V_i - V_j$ for node j. These matters will now be further explained.

4.1.1 Spring force

The point of departure is a beam which is replaced by a model as shown in Fig. 4.2, in which the mass of each segment and also the uniformly distributed load are concentrated in the hinges (the nodes). At a certain instant during the response the concentrated load is λf and λq respectively, where $\lambda f = mw_{,tt}$ and $m = \lambda\mu$ (the mass). It is to be noted

that the indices denoting position (x) and time (t) are omitted from the variables. Hence the moment is expressed by $M = M(x; t)$ in the continuous model and by $M_j = M_j(t)$ in the discrete model.

If a physically continuous beam, of constant flexural stiffness EI, is loaded by a constant bending moment, the curvature $\varkappa$ and bending moment M are linked by the following relation: $M = EI\varkappa$. If an angle Φ occurs between two adjacent segments in the deformed state in the discrete model, a moment $M = C\Phi$ will be acting at the hinge. The elastic spring constant C is so chosen that, for a constant moment, the hinges of the discrete model are located on the correct deflection curve which would occur for the actual continuous beam. Now $EI\varkappa = C\Phi$, where $\Phi = \varkappa\lambda$ (constant moment!). For the elastic spring constant we thus obtain $C = EI/\lambda$. (If the moment is not constant, the model will give an approximation of the actual condition).

The angle Φ which occurs between two segments can be expressed in the deflections w of the hinges, as is normally done in the finite-difference approach; see Fig. 4.3.

In the discrete model: $M_j = C_j \Phi_j = -EI(W_i - 2W_j + W_k)/\lambda^2$

In the continuous model: $M = EI\varkappa = -EIw_{,xx}$

Now consider the dynamic equilibrium of node j in the vertical direction; see Fig. 4.4. The shear forces V_i and V_j must support the concentrated load $\lambda(q - f)$ in accordance with the dynamic equilibrium equation (Newton's first law):

$$V_i - V_j = \lambda(q - f) \tag{21}$$

The elastic (spring) force in the continuous model, represented by the term $EIw_{,xxxx}$, is equal to the shear difference $V_i - V_j$ in the discrete model. In this way the fourth-order partial differential equation (continuous model) has been transformed into a number of ordinary differential equations of second order (discrete model). This number of equations is equal to the number of hinges in the model, and these differential equations

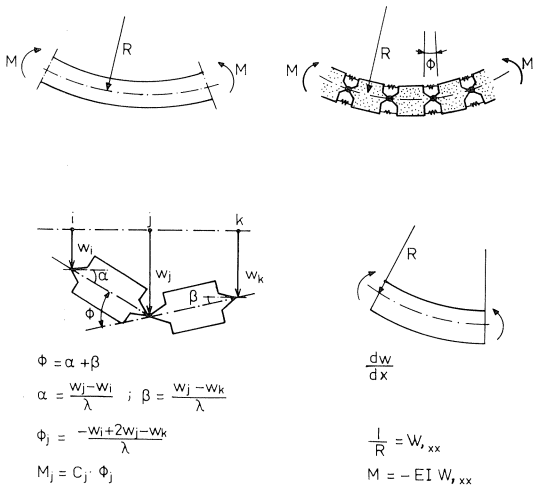

Fig. 4.3. The finite-difference analysis used in the discrete model as compared with the differential analysis.

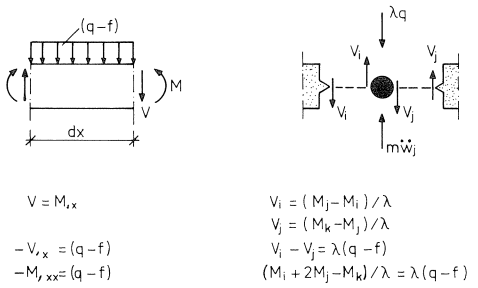

Fig. 4.4. Consideration of the vertical dynamic equilibrium.

must be solved simultaneously with respect to time. The differential equation of the continuous model is valid only in the elastic range. We shall now show that the set of differential equations of the discrete model is valid in the plastic range as well. By virtue of the relation existing between the moment M and shear force V formula (20) is equivalent to:

$$(-M_i + 2M_j - M_k)/\lambda = \lambda\,(q - f) \tag{22}$$

For each of these moments we already possess a relation linking them to the angular rotation $M = C\Phi$, where the rotation Φ is expressed in the discrete nodal deflections. The equilibrium equation is now *valid also in the plastic range.* This is apparent from formula (22) into which, after attainment of the plastic moment $M_p\,(= M_u)$ at a hinge, the plastic moment can be incorporated. The validity of the equation is not affected by this.

In order to calculate the plastic rotation Φ_{pu} correctly, we shall choose the length of each segment as equal to the depth of the beam. The maximum rotation for each hinge is approximately given by $\Phi_u = \varkappa_u \lambda$.

Note: The calculation with $\Phi_u = \varkappa_u \lambda$ must be regarded as an artifice. In the plastic behaviour range the curvature will not be constant over the length of the segment, but be concentrated in the "hinge" [27].

The angular rotation at which the plastic moment is attained at a hinge will be $\Phi_y = \varkappa_{sy} \lambda$. If the concrete section is asymmetrically reinforced, the value of Φ_y associated with a positive moment may therefore be different from that associated with a negative moment! For each hinge in the discrete model an M-Φ diagram can now be plotted.

From the foregoing it emerges that the moment at a hinge of the discrete model must be calculated on the basis of $M = C\Phi$ in the elastic range, while in the plastic range we have $M = M_p$.

In order to calculate the moment correctly during hysteresis it is necessary to extend the relation $M = C\Phi$. This will now be explained. A plastic hinge has developed, for which the moment M_p remains constant. At the instant when the angular rotation is

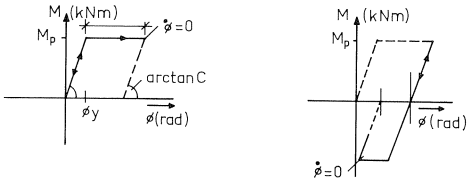

Fig. 4.5. Example of hysteresis applied in the discrete model.

about to decrease, which is manifested in a change of sign of the angular velocity $\dot{\Phi}$, the plastic hinges vanishes. The spring stiffness at the hinge is then once again equal to the elastic spring stiffness C; see Fig. 4.5. The relation $M = C\Phi$ is now not applicable in correctly calculating the moment; it would yield too large a moment. However, by subtracting the plastic rotation Φ_p from the rotation Φ it becomes possible again to calculate the moment correctly. So then:

$$M = C \cdot (\Phi - \Phi_p) \tag{23}$$

where Φ_p is the plastic angular rotation.

This relation is also valid in general if at $t = 0$ (t denotes time) the plastic angular rotation $\Phi_p = 0$. In the elastic range ($\Phi < \Phi_y$) the moment at the hinge is again equal to $M = C(\Phi - 0) = C\Phi$. When plastic yield has occurred and the angular velocity $\dot{\Phi}$ in the plastic range has changed its sign, the following holds: $M = C(\Phi - \Phi_p)$, where $\Phi_p \neq 0$.

4.1.2 Solving the differential equations

There are now sufficient known relations between the variables to enable the differential equations $V_i - V_j + m_j a_j = \lambda q(t)$ to be solved. Since there exists a non-linear relation between the moment M and the angular rotation Φ - bearing in mind the transition from the elastic to the plastic "branch" of the M-Φ diagram - the differential equation *must* be solved numerically for each hinge. For this purpose the DYNAMO program, operational at the Delft University of Technology, was employed. The name DYNAMO (derived from "*Dyna*mic *Mo*dels") denotes the compiler which translates continuous simulation models into higher programming languages (including Fortran and Algol). As a rule, only economic, sociological, psychological and biological systems used to be solved with DYNAMO. Later on, technically oriented problems were also dealt with, and it will emerge that our *exact* problem can likewise be solved with the aid of this program. DYNAMO can simultaneously solve a large number of non-linear first-order differential equations with respect to time. Hence the second-order differential equation has to be converted into a set of first-order differential equations. So, instead of $V_i - V_j + m_j a_j = \lambda q$, we have for node j (stating the time indices):

$$v_j(t) = \frac{d}{dt} w_j(t)$$

$$a_j(t) = \frac{d}{dt} v_j(t)$$

where the acceleration $a_j(t) = \{\lambda q(t) - V_j(t) + V_i(t)\}/m_j$

The set is solved with the aid of Euler's rule. For a time step Δt this gives:

$$w_j(t+\Delta t) = w_j(t) + \Delta t\, v_j(t) \tag{24}$$

$$v_j(t+\Delta t) = v_j(t) + \Delta t\, a_j(t) \tag{25}$$

where:

$$a_j(t) = \{\lambda q(t) - V_j(t) + V_i(t)\}/m_j \tag{26}$$

and where $q(t)$ is the given dynamic load.

In order to solve this set, initial conditions for the displacement w_j and velocity v_j must be given at time $t=0$. For example:

$t = 0$ $\quad w_j = 0$ or $w_j =$ static deflection
$v_j = 0$

Sufficient data are now available for calculating the variables (the solution) after the first time step. The values of the variables after the first time step are the initial conditions for the second time step. In general, a solution is obtained for each time interval Δt. This solution constitutes the initial conditions for the directly following time step, etc.

If a certain time duration of the response is considered, then, since this duration is divided into a large number of time intervals Δt, a large number of solutions will be known. These solutions represent the distribution of forces (V, M) at the hinges of the discrete model. After each time step we can test the distribution (M, V) for each hinge against the existing shear strength or rotational capacity calculated as indicated in Chapter 2.

4.1.3 Review of the calculation

Hinge j of the discrete model will be considered. At the instant t the discrete displacements, velocities and the load are known. In order to calculate the values of these variables at the instant $t+\Delta t$ we must solve the following three equations:

$$w_j(t+\Delta t) = w_j(t) + \Delta t\, v_j(t) \tag{24}$$

$$v_j(t+\Delta t) = v_j(t) + \Delta t\, a_j(t) \tag{25}$$

$$a_j(t) = \{\lambda q(t) - V_j(t) + V_i(t)\}/m_j \tag{26}$$

Equation (24) can be solved with the known displacement w_j and velocity v_j. In equation (25) a_j is still unknown. First, the shear difference $-V_j + V_i$ must be determined; see (26).

With the aid of the known displacements the following equations are successively solved:

$$\Phi_j(t) = \{-w_i(t) + 2w_j(t) - w_k(t)\}/\lambda \qquad \text{angle (27)}$$

$$M_j(t) = C_j\{\Phi_j(t) - \Phi_{jp}\} \quad \text{or} \quad M_j(t) = M_{jp} \qquad \text{moment (23)}$$

where $\Phi_{jp} = 0$ at $t = 0$; if $M_j(t) = M_{jp}$ and $\dot{\Phi} = 0$, then $\Phi_{jp} \neq 0$.

$$V_i(t) = \{M_j(t) - M_i(t)\}/\lambda \qquad \text{shear (28)}$$

$$V_j(t) = \{M_k(t) - M_j(t)\}/\lambda \qquad \text{shear (29)}$$

Substitution of the shear into (26) and of the acceleration $a_j(t)$ into (25) gives the velocity $v_j(t + \Delta t)$. Sufficient data are now known to enable the next time step to be calculated.

Also, after every time step the check calculations are performed, as indicated in Chapter 2. Check whether the *shear strength* is exceeded in the elastic range

$$V_{ju}(t) \geqslant \{V_j(t) + V_i(t)\}/2$$

The shear on the left of node j is different from that on the right of it. Therefore the average value is adopted at a node. The shear strength, as a function of the moment-shear combination, is equal to:

$$V_{ju}(t) = V_{jc}(t) + V_{jsv}$$

where:

$$V_{jc}(t) = \alpha_{jd}(t) V_{jn}$$

and:

$$\alpha_{jd}(t) = \alpha_{jd}\{M_j(t);\ V_j(t)\}$$

In the plastic range we must check for *rotational capacity:*

$$\Phi_{jpV} > \Phi_{jp}$$

i.e., the permissible plastic rotation > actual plastic rotation

$$\Phi_{jpV} = (1 - r_j)^2 \Phi_{jpu}$$

where $r_j = (\underline{V}_j - V_{jsv})/V_{jc}$ and $r_j = 0$ if $V_{jsv} \geqslant \underline{V}_j$.

$\underline{V}_j = (V_i + V_j)/2$ average shear force

The check for rotational capacity is applied only at the instant when $M_j = M_{jp}$!

4.2 *Non-constant stiffness of beam*

So far, the continuous beam has been assumed to have a constant flexural stiffness *EI*. It

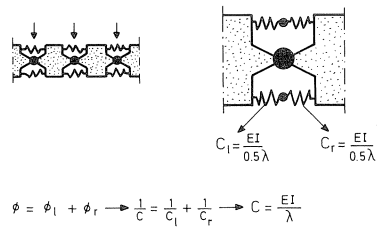

Fig. 4.6. Detail of a hinge in the discrete model.

will now be shown how a varying stiffness, due to differences in reinforcement, can be applied in the model.

By dividing the continuous beam into segments of length λ it can be represented by a discrete model in which the segments have been replaced by model portions, or elements, each of which is indeformable and is provided at each of its ends with a flexural spring having a spring constant $C_m = EI/\frac{1}{2}\lambda$. Flexural deformation is thus, as it were, concentrated at the two ends; see Fig. 4.6. C_m is therefore the flexural spring constant of *half* a segment. When two segments are connected to each other, two springs with constants C_l and C_r are connected in series. The new spring constant C of the two coupled springs is expressed by:

$$\frac{1}{C} = \frac{1}{C_l} + \frac{1}{C_r}$$

The spring characteristic for node j is determined by the adjacent segments on the left and right of node j and is equal to:

$$C_j = \frac{C_l C_r}{(C_r + C_l)}$$

In the special case of a beam with constant flexural stiffness EI we have $C_l = C_r = C_m = 2EI/\lambda$ and $C_j = EI/\lambda$.

4.2.1 Boundary conditions

An advantage of the approach described in Section 4.2 is that elastic restraint of the beam can be introduced in the same way. Consider a beam which is continuous over

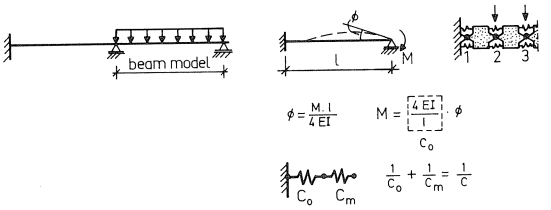

Fig. 4.7. Example of partial (elastic) restraint.

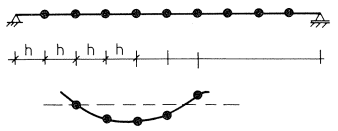

Fig. 4.8. The mass of the beam is distributed over the hinges, so-called "lumped mass" distribution.

three supports and is dynamically loaded on the right-hand span only, which alone will now be conceived as the discrete model. The left-hand span, which is not loaded, is replaced by a spring stiffness $C_0 = 4EI/l$, were l is the length of the span. The spring stiffness C_0 is equal to the bending moment which occurs at the intermediate support when an angular rotation of 1 radian occurs there. The flexural spring constant C_m of the adjacent half segment is:

$$C_m = EI/\tfrac{1}{2}\lambda.$$

The total flexural spring stiffness of the node is:

$$\frac{1}{C} = \frac{1}{C_0} + \frac{1}{C_m}$$

For the general case of a *partial restraint* this therefore gives:

$$C = \frac{C_0 C_m}{(C_0 + C_m)}$$

For a *hinged bearing* (no flexural restraint): $C = 0$ $(C_0 = 0)$
For a *fixed end* (complete restraint): $C = C_m$

In general, for the spring characteristic C comprising two coupled springs C_0 and C_m, the following relation exists:

$$\frac{1}{C} = \frac{1}{C_0} + \frac{1}{C_m}$$

At a fixed end we have $C_0 = \infty$, and therefore $C = C_m$. If the beam has a constant flexural stiffness EI, then $C_m = EI/\tfrac{1}{2}\lambda$. Therefore $C = 2EI/\lambda$; and for another node j we have $C_j = EI/\lambda$. Hence the spring stiffness at a fixed end is evidently $C = 2C_j$.

4.3. *Limitation of the mathematical model*

As has been discussed in the preceding section of this chapter, the continuous beam is divided into segments of length λ. In order to calculate correctly the plastic rotation which occurs at a hinge, the length λ of a segment should be chosen approximately equal to the depth h of the beam. A direct consequence of the above schematization is that the masses of the segments, concentrated in the hinges, are located at distances h from one another.

On comparing the behaviour of a beam schematized in this way with that of a beam analysed by the finite-element method ("lumped mass" conception), the response is found to be quite reasonably accurate, provided that the natural frequencies are not too high [46]. A rule of thumb in using a "lumped mass" matrix is to try to locate at least three point masses between two vibration nodes (the wavelength) [47]. Although the finite-element analysis presupposes an *elastic* response, we shall assume this rule of thumb to be applicable also to our model, i.e., including a plastic response.

4.3.1 Flexural theory

The starting point chosen for our discrete model is a beam which, when loaded perpendicularly to its axis, undergoes only a deformation due to bending within the plane of loading. The vibration modes with high frequencies will, as also in other structures, be associated with short wavelengths. This means that the ratio between the depth of the beam and the length of deflection curve will soon no longer be negligibly small, as is required in applying conventional flexural theory. In consequence, for higher frequencies the shear deformation and rotational behaviour will have to be brought into the analysis. So the mathematical model employed here is valid only for forced vibrations with sufficiently low loading frequencies. Only then it is permissible to neglect shear deformation and rotational inertia.

5 Worked examples

The discrete model described in the preceding chapter is used for analysing the elasto-plastic response of beam loaded by a uniformly distributed impulsive load.

Two different examples will be considered. The first is concerned with the response of a simple-supported beam, while the second describes the behaviour of a beam fixed at its ends. The example of the simply-supported beam has been chosen in order to be able to explain experimental results. Thus it has been found in tests that in beams subjected to a uniformly distributed pulse-type load often no plastic hinges are formed or that failure occurs at mid-span. In most cases, however, plastic hinges were formed or failure occurred at a section located close to the support. The second example, the fixed-end beam, approximately represents a strip of the roof of an immersed-tube road tunnel, and the situation associated with a gas explosion in the tunnel will be considered. It will more particularly be determined what load capacity the beam (the strip) has under dynamic combinations of moment and shear.

5.1 *Simply-supported beam*

The beam will be assumed not to fail in shear, i.e., sufficient shear reinforcement has been provided. The required quantity of shear reinforcement is determined after the response has been calculated. The beam has a span of 15 m and a depth $h = 1.2$ m (effective depth $d = 1.15$ m); its width is 1 m. A low reinforcement percentage has been adopt-

ed, namely, 0.3% for both tensile and compressive reinforcement. A yield moment is assumed to occur at a concrete section at between 0.01 s and 0.1 s. Then the average dynamic material properties, as determined in Section 3.4. of this report, are applicable. For concrete grade B 22.5 and steel grade FeB 400 this leads to the following material data:

- reinforcing steel: $f_{syd} = 1.25 \times 400 = 500$ N/mm^2
  $E_{sd} = 2.1 \times 10^5$ N/mm^2
  $\varepsilon_{su} = 10\%$
- concrete $f_{cd} = 22.5$ N/mm^2
  $f_{ctd} = 1.3 \times 1.85 = 2.40$ N/mm^2
  $E_{cd} = 1.3 \times 28000 = 36400$ N/mm^2
  $\varepsilon_{cu} = 0.175\%$

With the aid of these data the plastic moment M_p, the curvatures $\varkappa_{sy}$ and $\varkappa_u$ and the dynamic shear force V_{cd} resisted by the concrete can be calculated:

$M_p \quad (= M_u) = 1932$ kNm
$\varkappa_{sy} \quad = 2.46 \times 10^{-3}$ 1/m
$\varkappa_u \quad = 24.25 \times 10^{-3}$ 1/m
$M/Vd < 0.75$:
$V_{cd} = 0.67 \times 2.40 \times 1 \times 1200 = 1930$ kN
$M/Vd > 1.75$:
$V_{cd} = \alpha_d V_n$

$$V_n = 22.5^{1/2} \times 0.3^{1/3} \times 1150^{3/4} \times 1 \times \left(\frac{2.40 + 1.85}{2 \times 1.85}\right) 0.83 = 598 \text{ kN}$$

In order to convert the physically continuous beam into the discrete mathematical model, it is divided into segments, each of which should have a length approximately equal to the depth of the beam so that the plastic rotation Φ_{pu} will be correctly taken into account. We shall therefore choose 12 segments, each with a length $\lambda = 1.25$ m. Now the moment-angle (M-Φ) relation can be determined for each hinge in the discrete mathematical model.

$\Phi_y = \varkappa_{sy} \lambda \quad = 2.46 \times 10^{-3} \times 1.25 = 3.08 \times 10^{-3}$ rad
$\Phi_u = \varkappa_u \lambda \quad = 24.25 \times 10^{-3} \times 1.25 = 30.31 \times 10^{-3}$ rad
$\Phi_{pu} = \Phi_u - \Phi_y = 27.23 \times 10^{-3}$ rad

Here Φ_{pu} is the maximum plastic rotation if the actual shear force is zero or is resisted entirely by shear reinforcement. If a shear force is present and insufficient shear reinforcement is provided, the maximum *permissible* plastic rotation Φ_{pV} can be calculated with the aid of formula (14).

5.1.1 Load

The continuous beam carries a uniformly distributed impulsive load of 4.8 kNs/m. In the discrete mathematical model of the beam this load is replaced by an equivalent set

of dynamic point loads. Each hinge is now loaded by a pulse of $4.8 \times 1.25 = 6$ kNs at the instant $t = 0$. The concentrated mass m of each hinge is 3600 kg, so that each hinge acquires an initial velocity v due to the impulsive load, namely, $v = 6000 : 36000 = 1.6\dot{6}$ m/s. The analysis could be conceived as an experiment in which the beam is allowed to fall freely from a certain height so as to land on its supports at the instant $t = 0$.

For solving the differential equations the initial conditions at $t = 0$ for the displacements w and velocity v must be known; see also Section 4.1.2. The velocity v can be taken as zero for each spring (one time step later the velocity is $v = 1.6\dot{6}$ m/s). The initial displacement, i.e., the static deflection of the discrete mathematical model, can be expressed in the static load $F_{stat} (= 36$ kN) and the spring stiffness C. The latter is obtained from:

$$C = M_p/\Phi_y = 1932 : 3.08 \times 10^{-3} = 627000 \text{ kNm/rad}$$

At the instant $t = 0$ the discrete hinge displacements are:

$$w_2 = w_{12} = 71.5 \text{ B} \qquad w_5 = w_9 = 236.5 \text{ B}$$
$$w_3 = w_{11} = 137.5 \text{ B} \qquad w_6 = w_8 = 262.5 \text{ B}$$
$$w_4 = w_{10} = 193.5 \text{ B} \qquad w_7 = 271.5 \text{ B}$$

where the constant $B = (\lambda^2 F_{stat})/C = 8.97 \times 10^{-5}$ m

Sufficient data are now known for carrying out the response analysis. A number of results of the dynamic calculation are given in Fig. 5.2.

5.1.2 Results

Fig. 5.2 shows the moment and shear diagrams (M and V) for the beam as a whole at various times t. This analysis is conceived as corresponding to the "experiment", mentioned earlier on, in which the beam is allowed to fall freely from a certain height. For very short (early) times the beam "hardly notices" that it has landed on its supports. Only at the ends of the beam are marked extra curvatures produced and will extra moments therefore occur. Large shear forces are likewise produced in this part of the beam. At later points of time the bending moment diagram changes its shape. A closer inspection of the shear diagrams clearly reveals that a shear wave travels along the beam. In conformity with the bending moment behaviour it is seen that plastic hinges are formed at some distance from the supports and then move towards mid-span! This behaviour is in agreement with the available results of experiments. Also, a displacement w and some moment M and shear forces V as functions of time are shown in

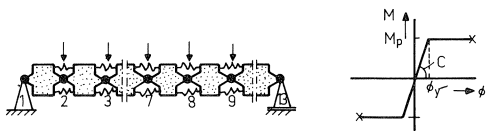

Fig. 5.1. The flexural beam composed of 12 infinitely rigid segments connected to each other by flexural springs. The M-Φ diagram required for these springs is shown on the right.

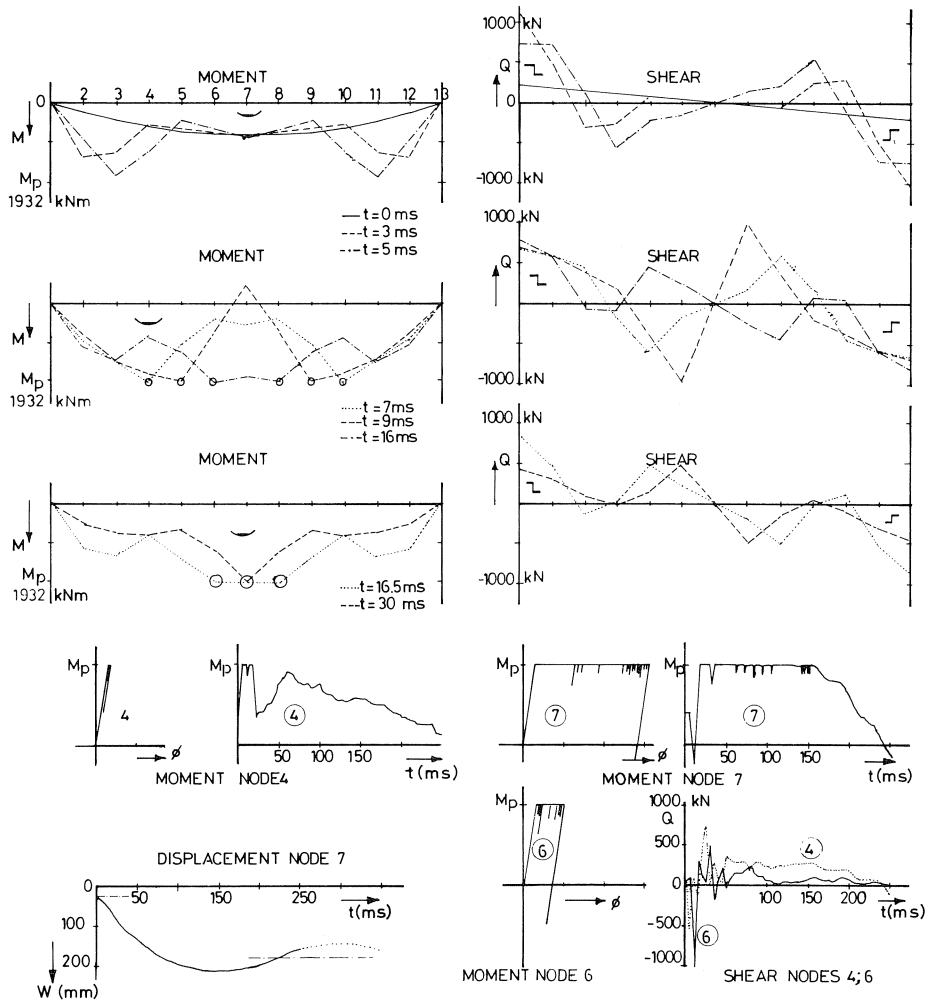

Fig. 5.2. Some characteristic diagrams for a simply-supported beam subjected to a uniformly distributed impulsive load.

Fig. 5.2, which moreover shows - in the elasto-plastic M-Φ diagrams - how the moment-angle relation has been conformed to. The M-Φ diagrams clearly reveal that a plastic hinge develops, vanishes, and may form again at the *same* hinge location. It will now briefly be indicated how the maximum permissible plastic rotation Φ_{pV} is calculated in the model.

5.1.2.1 Rotational capacity

The effect of the shear force V on the plastic rotation is expressed by formula (14):

$$\Phi_{pV} = (1 - r)^2 \Phi_{pu} \quad \text{where} \quad r = (V - V_{sv})/V_{cd}$$

By carrying out the analysis on the assumption that there is no shear reinforcement, i.e., for $V_{sv} = 0$, we can determine, with the aid of the calculated results - such as, among others, the factor $r (= V/V_{cd})$ - how much shear will have to be resisted (V_{sv}) by separate shear reinforcement. Now consider hinge 4. As shown in Fig. 5.2, the first plastic hinge is formed at $t = 7$ ms. At that instant the factor $r = 0.58$. With the aid of formula (14) the maximum plastic rotation Φ_{pV} can be calculated, giving:

$$\Phi_{pV} = (1 - 0.58)^2 \times 27.23 \times 10^{-3} = 4.80 \times 10^{-3} \text{ rad}$$

The plastic hinge at node 4 is present from $t = 7$ ms to $t = 7.4$ ms. After $t = 7.4$ ms the moment decreases ($M < M_p$). The plastic rotation Φ_p that has occurred is equal to 0.09×10^{-3} rad. Now this rotation Φ_p must be less than the permissible plastic rotation Φ_{pV}, i.e.:

$$\Phi_p < \Phi_{pV} \quad \text{or} \quad 0.09 \times 10^{-3} < 4.80 \times 10^{-3}!$$

The rotational capacity of the beam is therefore adequate.

At the instant $t = 11.5$ ms a plastic hinge again occurs, as is clearly seen in Fig. 5.2, where the moment at node 4 is represented as a function of time. The factor r is now calculated afresh, because the shear force varies as a function of time. From the program output (not given) follows $r = 0.36$. This gives:

$$\Phi_{pV} = (1 - 0.36)^2 \times 27.23 \times 10^{-3} = 11.15 \times 10^{-3} \text{ rad}$$

The plastic hinge is now present from $t = 11.5$ ms to $t = 12.5$ ms. Then the moment decreases and remains within the elastic range. The total plastic rotation Φ_p that occurs is 0.26×10^{-3} rad. Again the rotational capacity of the beam is found to be adequate ($0.26 \times 10^{-3} < 11.15 \times 10^{-3}$). The beam will therefore not fail due to lack of rotational capacity at hinge 4.

In this way the hinges where plastic moments occur are checked. In the present instance these are the hinges 4 (= 10), 5 (= 9), 6 (= 8) and 7. Some important output results are summarized below.

plastic hinge 4			plastic hinge 5			plastic hinge 6			plastic hinge 7		
r	Φ_{pV}	Φ_p	r	Φ_{pV}	Φ_p	r	Φ_{pV}	Φ_p	r	Φ_{pV}	Φ_p
0.58	4.80	0.09	0.93	0.13	0.17*	0.63	3.78	0.38	0.00	27.23	11.87
0.36	11.15	0.26	0.19	17.87	0.80	0.06	24.06	1.87	0.37	10.81	12.74*
			0.14	20.14	1.00	0.15	19.67	2.05	0.03	25.62	13.18
			0.29	13.73	1.46	0.14	20.13	2.47	0.00	27.23	16.11
			0.53	6.02	1.69	no failure			no failure		
			0.57	5.03	1.78						
						0.22	16.57	7.36	0.06	24.06	25.92*
						0.18	18.31	7.41	0.16	19.21	26.31*
						0.25	15.32	7.45	0.24	20.69	26.69*
									0.41	9.48	27.22*

* failure of the section $\Phi_p > \Phi_{pV}$

Φ_p and Φ_{pV} to be multiplied by 10^{-3}

From this summary it emerges that failure occurs at the hinges 5 and 7. The rotational capacity is therefore not sufficient. It is to be noted that for hinge 7 a different calculation procedure has been followed. From considerations of symmetry it is apparent that at node 7 the average shear force $(V_6 + V_7)/2$ will be zero. The factor r is, accordingly, always zero and therefore the maximum plastic rotation would always be permissible: $\Phi_{pV} = \Phi_{pu}$! This appears improbable. For this reason we shall take a closer look at hinge 7; see Fig. 5.3.

The physically continuous beam has been divided into a number of segments of length λ. At the hinges the average behaviour of a small beam portion of length λ is calculated - or, more precisely, at a hinge the average behaviour of half the adjacent segments is considered. Hinge 7 therefore describes the behaviour of the half segments 6 and 7; see Fig. 5.3. The plastic rotation is conceived as concentrated in the hinge. In reality, however, this plastic rotation will be distributed over a certain length of the beam. Hence, in our case, a plastic rotation will occur directly beside hinge 7 and will therefore weaken the beam section. But a shear force is present directly beside hinge 7 and may, if large plastic deformations occur, give rise to failure. For this reason we shall, at hinge 7, adopt as the measure for the shear force the value which occurs at a distance $0{,}25\lambda$ from this hinge. This value is equal to V6/2, i.e., half the shear force that occurs in segment 6!

From the summary of results given above it appears that the beam fails at hinges 5 and 7. The rotational capacity can be improved by providing shear reinforcement.

Example:
For hinge 7 we have $r = 0.41$, $\Phi_{pV} = 9.48 \times 10^{-3}$ rad, $\Phi_p = 27.22 \times 10^{-3}$ rad (see summary). At the same instant when the factor $r(= 0.41)$ has been calculated there occurs a shear force $V(= \frac{1}{2}V6) = 192$ kN. The concrete itself can transmit 468 kN $(= V_{cd})$. The *entire* shear force that occurs will be resisted by shear reinforcement. Then:

$$r = \frac{V - V_{sv}}{V_{cd}} = \frac{192 - 192}{468} = 0$$

This means that the rotational capacity is now of maximum magnitude, therefore $\Phi_{pV} = \Phi_{pu}$!

A comparable calculation can be carried out for hinge 5: $r = 0.93$, $\Phi_{pV} = 0.13 \times 10^{-3}$ rad, $\Phi_p = 0.17 \times 10^{-3}$ rad (see summary). These values have been calculated at $t = 9$ ms.

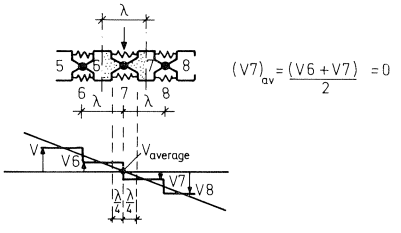

Fig. 5.3. Hinge 7 and the shear diagram considered in detail.

From Fig. 5.2 we obtain for the shear force that occurs: $|V5| = +445$ kN; $V5 = 0.93 \times 4V_{cd}$ and therefore $V_{cd} = 478.5$ kN.

Now the following must be satisfied:

$$(1-r)^2 \Phi_{pu} \leqslant 0.17 \times 10^{-3} \text{ rad } (\Phi_{pu} = 27.23 \times 10^{-3} \text{ rad})$$

Hence it follows that $r \leqslant 0.92$ and $V_{sv} \geqslant 4.8$ kN. This value is of no practical significance in the present case, but does illustrate how the output results are processed.

5.1.2.2 Shear strength

For each time step the model calculates the actual forces that occur, such as moments M and shear forces V, and the shear V_{cd} that can be resisted. In Fig. 5.4 the ratio V/V_{cd} has been plotted for a number of hinges. If this ratio is larger than 1, shear failure occurs. In the left-hand diagrams the actual shear force V4 and the ratio $V4/V_{cd}4$ for the first 60 ms are represented on a larger scale. The highest value of the ratio, namely 1.28, occurs at the instant $t = 23$ ms. The shear force V4 is then equal to 688 kN.

The concrete itself resists a force 538 kN (688 : 538 = 1.28). So this means that 688 − 538 = 150 kN has to be resisted by shear reinforcement (V_{sv}). It is to be noted that at the instant when a plastic moment M_p *is formed* at hinge 4 the ratio $V4/V_{cd}4$ is equal to the factor r needed for calculating the permissible rotational capacity. In our case a plastic moment M_p4 is formed at $t = 7$ ms and $t = 11.5$ ms, the factor r being 0.58 and 0.36 respectively.

A comparable calculation can be carried out for node 5, giving:

$$t = 7.5 \text{ ms} \qquad V5/V_{cd}5 = 1.18 \qquad V5 = -615 \text{ kN} \qquad V_{cd} = -521 \text{ kN}$$

Shear reinforcement V_{sv} must resist a force of 615 − 521 = *94 kN*. If the shear force is resisted by separate stirrup reinforcement, the quantity of such reinforcement can be calculated with the aid of the truss analogy. With vertical stirrups the quantity of stirrup

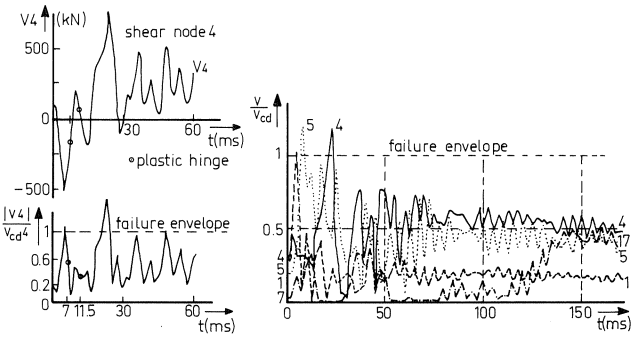

Fig. 5.4. The ratio V/V_{cd} for some hinges and, shown on the left, the shear force V4 and ratio $(V/V_{cd})4$ for hinge 4.

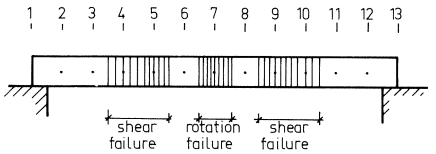

Fig. 5.5. The zones of the beam where shear reinforcement is needed are indicated; also the reason why.

reinforcement per unit length is obtained from:

$$\frac{A_{sv}}{t} = \frac{V_{sv}}{f_{syd} \times z} = \frac{V_{sv}}{f_{syd} \times 0.85 \times d} \text{ (mm}^2\text{/mm)}$$

where t denotes the stirrup spacing and A_{sv} the stirrup cross-sectional area in mm^2. For hinges 4 and 5 this calculation results in the following quantities of stirrup reinforcement per unit length:

hinge 4: $\frac{A_{sv}}{t} = \frac{150 \times 10^3}{500 \times 0.85 \times 1150} = 0.31$ mm^2/mm 8 mm stirrups at 323 mm centres

hinge 5: $\frac{A_{sv}}{t} = \frac{94 \times 10^3}{500 \times 0.85 \times 1150} = 0.19$ mm^2/mm 8 mm stirrups at 526 mm centres

The theoretical quantity of stirrup reinforcement as calculated is very small. It should be borne in mind, however, that only a very low reinforcement percentage of 0.3% has been provided in this deep beam. With higher reinforcement percentages not only the yield moment increases, but also the dynamically occurring shear force. In consequence, the quantity of stirrup reinforcement required will increase rapidly, also because V_{cd} increases only slowly. The beam is shown in Fig. 5.5, indicating where shear reinforcement is needed.

5.1.3 Concluding remarks

Depending on the cross-sectional dimensions of the beam, the strength of the concrete, the strength of the reinforcing steel, the percentage of reinforcement and the magnitude of the impulsive load applied, different responses will be found. If the impulse applied is small, an elastic response will be obtained at all instants of time. With increasing magnitude of the impulse the first plastic hinge will be formed at mid-span. With further impulse increase the response will become as described in this example, and if it increases still further, failure of the beam will occur in consequence of the rotation Φ_u being exceeded.

5.2 *Beam fixed at both ends*

This example is associated with research into the question whether explosive substances are allowed to be transported through road tunnels. Interest is more particularly focused on the behaviour of the roof of the tunnel in the event of its being subjected to

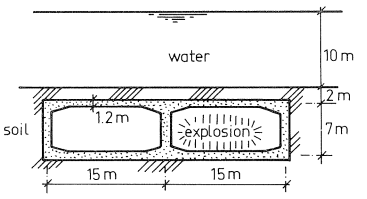

Fig. 5.6. An example of a road tunnel under a waterway, as constructed in the Netherlands.

load from an explosion. A 1 m wide strip of the roof will be considered. This beam (the strip) which is conceived as fixed (fully restrained) at both ends is representative of the response of the tunnel roof if an explosion occurs in the tunnel. Fig. 5.6 shows a cross-section through a tunnel of this kind, which is the type commonly employed in the western part of the Netherlands. It is a submerged or immersed-tube tunnel installed under a 2 m thick soil cover and a 10 m depth of water. The span is 15 m and the roof is 1.2 m thick. In this example, too, the beam is divided into 12 segments, so that $\lambda =$ 1.25 m.

5.2.1 Load

Fig. 5.7 shows a pressure-time diagram of the shock wave (detonation) due to an explosion in a tunnel. In this diagram p_{max} is the peak excess pressure (overpressure), expressed in bars (1 bar = 100 kN/m^2), and t_d is the length of time during which the pressure exists (positive phase). After $t = t_d$ a suction will occur (negative phase). The pressure-time diagram is expressed with fair accuracy by the following formula:

$$p(t) = p_{max}\left(1 - \frac{t}{t_d}\right) e^{-\alpha \frac{t}{t_d}}$$

The coefficient α is a shape factor of the shock wave. In a tunnel it can be taken as having a value of 4. Depending on the type of liquefied gas giving rise to the explosive mixture in the tunnel, the peak pressure ranges from 10 bar to as much 25–30 bar. Tests have been performed in scale models of tunnels which show that the positive phase t_d is of about 50 ms duration. It is not quite clear what model laws should be used in order to determine the value t_d in an actual tunnel, t_d can be expected to become larger. For this reason the effect of three values of t_d – 50 ms, 100 ms and 150 ms respectively – upon the response was investigated.

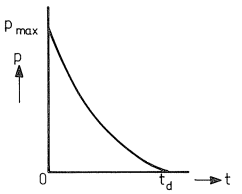

Fig. 5.7. Pressure-time diagram for an explosion in a tunnel.

The static load is directly determinable from the location of the tunnel; see Fig. 5.6. The roof is loaded by 10 m of water and 2 m of soil as well as the dead weight of the roof itself. The resulting static load is: $10 \times 10 + 1.2 \times 24 + 2 \times 19 = 100 + 28.8 + 38 = 166.8$ kN/m. This uniformly distributed load is converted into an equivalent set of point loads. Each hinge is subjected to a static load of $166.8 \times 1.25 = 208.5$ *kN*.

The mass of the water and of the soil must also be introduced into this analysis. In this case the entire mass of the water and soil over a segment is concentrated in the hinge. To the mass m of 3600 kg (concrete) is added 17250 kg (water, soil), so that the total mass at a hinge is $m = 20850$ kg.

At the instant $t = 0$ the following discrete hinge displacements can be calculated:

$$w_2 = w_{12} = 5.96 \text{ B} \qquad w_5 = w_9 = 45.33 \text{ B}$$
$$w_3 = w_{11} = 18.33 \text{ B} \qquad w_6 = w_8 = 53.96 \text{ B}$$
$$w_4 = w_{10} = 32.63 \text{ B} \qquad w_7 = 57.00 \text{ B}$$

where the constant $\text{B} = (\lambda^2 F_{\text{stat}})/C$.

First, a beam fixed at both ends is considered, assuming no shear failure to occur. We shall begin with a high percentage of symmetrically placed reinforcement, namely 1.8%. In order to investigate the effect of the changing material properties, the response of the tunnel roof will be calculated both for *static* and for *dynamic* material properties. For the dynamic properties it will again be assumed that the yield moment occurs at a concrete section within 0.01 s to 0.1 s. The dynamic material properties are thus the same as those adopted in the previous example. Now again the beam is divided into 12 segments, each $\lambda = 1.25$ m in length. The following values are obtained for the M-Φ relation:

$$M_p = 10605 \text{ kNm } (8665 \text{ kNm})$$
$$\Phi_y = 3.90 \times 10^{-3} \text{ rad } (3.76 \times 10^{-3} \text{rad})$$
$$\Phi_u = 8.54 \times 10^{-3} \text{ rad } (33.00 \times 10^{-3} \text{rad})$$

The values calculated on the assumption of normal static material properties are given in parentheses. At the fixed end:

$$\Phi_y(\text{fixed end}) = \tfrac{1}{2}\Phi_y = 1.95 \times 10^{-3} \text{ rad } (1.88 \times 10^{-3} \text{ rad})$$

The principal difference to emerge from a comparison between the results calculated with different material properties is that the results rotation Φ_u is reduced to a quarter when the dynamic properties are adopted. This is a direct consequence of the reduction of the compressive strain of the concrete, which is halved ($\varepsilon_{cu,dyn} = 0.175\%$, $\varepsilon_{cu,\text{stat}} = 0.35\%$).

5.2.2 Results

We begin with the analysis of a fixed-end beam which will restrict itself to checking whether the maximum rotational capacity Φ_u is exceeded. Hence it is provisionally assumed that adequate shear strength is ensured. The analysis arrives at the following results for this beam:

$\varrho_s = 1{,}8\%$

t_d	p_{max} (rotational capacity) dynamic material properties	static material properties
50 ms	36 bar	57 bar
100 ms	20 bar	32 bar
150 ms	16 bar	23 bar

It emerges that if the response is calculated with static material properties the permissible load p_{max} is approximately 1.5 times as large as p_{max} when the dynamic material properties are used in the calculation. This is directly due to the difference in the maximum rotational capacity Φ_u. The latter decreases if the loading rate is increased, because then ε_{cu} decreases. It further appears that p_{max} decreases with increasing magnitude of t_d. As a (rough) approximation the product of p_{max} and t_d can be taken as constant. In other words, the total impulse is more or less the governing quantity for the magnitude of the permissible explosion load. In the response calculation it is found that, for each value of t_d, the plastic hinges at the fixed end and at mid-span are formed in the same manner way as under static load (different from the response in a simply-supported beam!). Fig. 5.8 shows some characteristic diagrams for the response of a tunnel roof subjected to an explosion load $p_{max} = 16$ bar and $t_d = 150$ ms. The fixed-end moment soon acquires a value M_p which remains constant for some time and then, after a further time, changes its sign. The complete hysteresis loop associated with this behaviour is well displayed in the M-Φ diagram for node 1. The plastic moment M_p occurs at mid-span only once and for a short time. After that, the vibration of this part of the beam die away elastically.

The M-Φ diagrams of nodes 1 and 7 show that the plastic rotation at the fixed ends is greatest and therefore constitutes the governing criterion for the permissible explosion load. The shear forces fluctuate rather more, but not as much as in the simply-supported beam. The principal reason for this is the greater mass of the fixed-end beam, since the mass of the water and soil over the tunnel roof is additional to that of the beam itself.

The diagrams also clearly show that large shear forces can occur at points along the beam (nodes 5 and 6) where a static load would produce only a small shear force! The mid-span displacement w as a function of time is also shown in Fig. 5.8. As a result of plastic behaviour a permanent deformation will occur, as shown by the dotted curve. It can be concluded that the diagrams for displacement and bending moment correspond to the response that a single-mass spring system would give. However, such a spring system is not suitable for calculating shear forces.

The calculations do give insight into the response, but are of no practical value because the shear forces obtained are far too large (5000 kN). In tunnel roofs without shear reinforcement the permissible nominal shear stress τ_u is approximately 1 N/mm^2, whereas values of between 5 and 7 N/mm^2 are found. The starting point that the sufficient shear strength is ensured therefore turns out to have been incorrect. The permissible p_{max} will

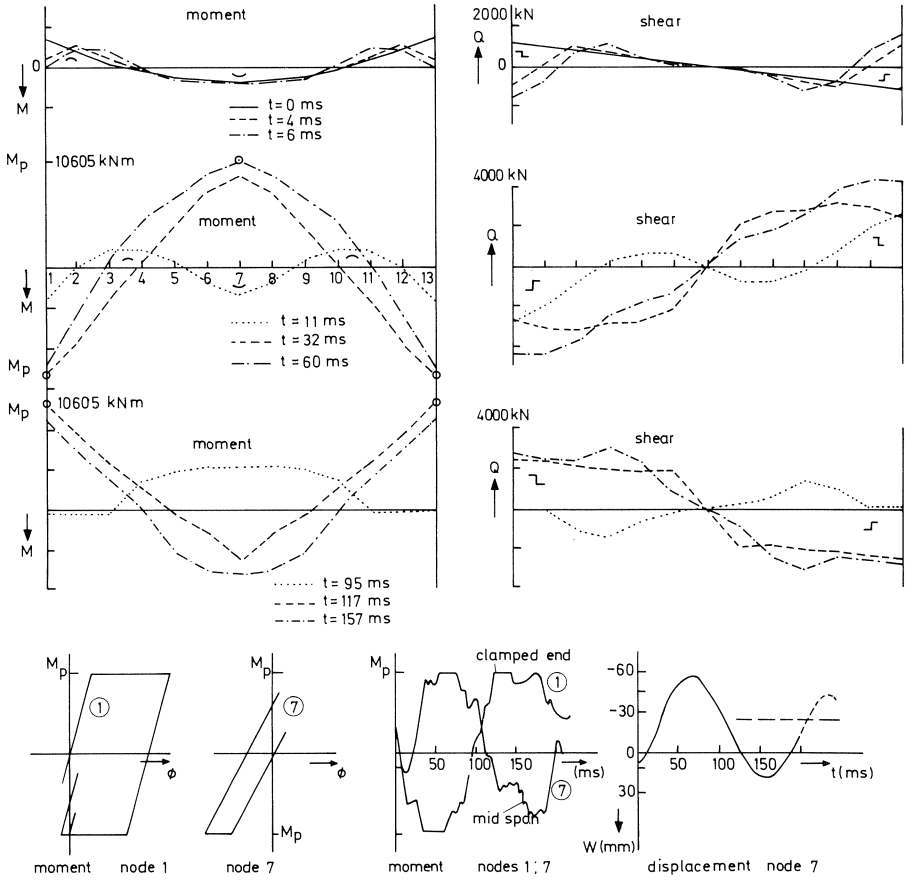

Fig. 5.8. Response of a tunnel roof to an explosion load.

actually be much lower. In order to reveal the effect of the shear failure criterion a fresh analysis was performed, in which the haunches at the ends of the beam were also taken into account so as to simulate the tunnel roof more closely; see Fig. 5.9. Response calculations were carried out for various reinforcement percentages: 0.7%, 1.1%, 1.8% and 2.5%. Only the results obtained for $\varrho_s = 1.1\%$ will be given here. The following input data were used in the calculations:

node 1:	$M_p = +\ 8900$ kNm	$\Phi_y = +1.38 \times 10^{-3}$ rad	$\Phi_u = +8.63 \times 10^{-3}$ rad
	$M_p = -12750$ kNm	$\Phi_y = -0.86 \times 10^{-3}$ rad	$\Phi_u = -5.57 \times 10^{-3}$ rad
	$M/Vd > 1.75$	$V_n = +1480$ kN	$V_n = -1522^*$ kN
	$M/Vd < 0.75$	$V_{cd} = \pm 3861$ kN	
node 2:	$M_p = +\ 7850$ kNm	$\Phi_y = +3.77 \times 10^{-3}$ rad	$\Phi_u = +7.02 \times 10^{-3}$ rad
	$M_p = -10905$ kNm	$\Phi_y = -3.48 \times 10^{-3}$ rad	$\Phi_u = -5.03 \times 10^{-3}$ rad
	$M/Vd > 1.75$	$V_n = +1474$ kN	$V_n = -1522^*$ kN
	$M/Vd < 0.75$	$V_{cd} = \pm 2800$	

* Including stirrup force in haunch.

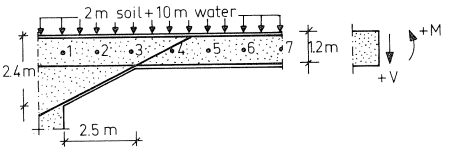

Fig. 5.9. Section through a half tunnel roof with haunch; the manner in which positive forces (M, V) act on the section is shown on the right.

nodes 3 to 7:

$M_p = \pm 6565$ kNm $\quad \Phi_y = \pm 3.56 \times 10^{-3}$ rad $\quad \Phi_u = \pm 11.94 \times 10^{-3}$ rad

$V_n = \pm 911$ kN $\quad V_{cd} = \pm 1930$ kN

At the instant $t = 0$ the discrete nodal displacements are:

$w_2 = w_{12} = 1.66$ B $\quad w_5 = w_9 = 26.71$ B

$w_3 = w_{11} = 7.90$ B $\quad w_6 = w_8 = 33.29$ B

$w_4 = w_{10} = 17.41$ B $\quad w_7 = 35.65$ B

where $B = 1.77 \times 10^{-4}$ m ($F_{stat} = 208.5$ kN; m = 20850 kg).

The results of the dynamic response analysis of the tunnel roof (without shear reinforcement) are as follows:

$\varrho_s = 1.1\%$

t_d	p_{max} (rotational capacity)	p_{max} (shear failure)
50 ms	31 bar	5.0 bar
100 ms	17 bar	3.5 bar
150 ms	13 bar	2.5 bar

As a result of bringing in the shear failure criterion the permissible value of p_{max} is thus seen to have been drastically reduced as compared with the situation where it is merely checked whether the *maximum* rotational capacity is exceeded. Broadly speaking, it can be said that p_{max} decreases to one-fifth of the earlier value. For higher percentages of reinforcement the reduction will be even greater!

On considering the results for $p_{max} = 2.5$ bar (Fig. 5.10) it is found that even no plastic moments now occur! At a higher load shear failure will be take place before a plastic moment can develop. Although the distribution of the bending moment along the span is similar in shape to that obtained under static load, the shear force distribution is quite different. Shear failure occurs not only at node 3, but also at note 5 or 6, i.e., close to mid-span! Furthermore, the results indicate that the largest shear forces occur at the instant when the tunnel roof has fallen back and has reached its lowest point. The mid-span displacement (node 7) has been plotted as a function of time in Fig. 5.10. It follows from this diagram that the tunnel roof is "lifted" hardly any higher than the zero axis in the diagram. A more powerful explosion will "lift" the roof higher, so that it will fall back from a greater height. When it has thus fallen back, the roof will fail in shear in conse-

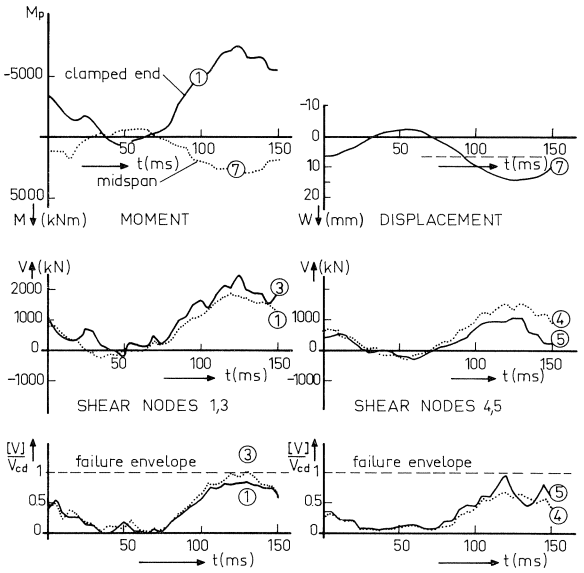

Fig. 5.10. Some moment and shear diagrams, the displacement-time diagram and the relative shear force; $p_{max} = 2.5$ bar and $t_d = 150$ ms.

quence of the larger shear forces that develop. So the "falling back" of the tunnel roof is the governing aspect with regard to its strength!

The calculations for $t_d = 150$ ms were carried out also for the other above-mentioned reinforcement percentages. Surprisingly, the permissible value for p_{max} in all cases was found to be 2.5 bar! Although the permissible shear force increases with higher reinforcement percentage, the shear force that actually occurs evidently also increases as a result of an increase in flexural stiffness.

Although shear reinforcement is not normally installed in tunnel roofs, it will nevertheless be necessary to find some way of resisting larger shear forces. Only then will it be possible to increase the permissible value of p_{max}. It might be possible, without having recourse to stirrups, to increase the shear strength by providing an extra layer of reinforcement in the middle plane (i.e., at mid-depth) of the tunnel roof slab (Fig. 5.11). When shear failure has occurred, this additional longitudinal reinforcement will hold the two parts, separated by the fracture, tightly together, so that shear force can still be transferred by aggregate interlock and dowel action. The shear strength attained can be calculated as follows:

$$\tau_{ud} = 1.4 + 0.8\varrho f_{std}$$

Additional longitudinal reinforcement amounting to 0.5% in the middle plane of the roof slab provides a shear strength $\tau_{ud} = 3.5$ N/mm^2, enabling $p_{max} = 13$ bar and $t_d = 150$ ms to be resisted. Plastic hinges can now also develop again. Another possibility consists in the application of steel-fibre-reinforced concrete. With high percentages of steel fibres (2%) it is likewise possible to resist $p_{max} = 13$ bar and $t_d = 150$ ms.

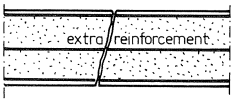

Fig. 5.11. Extra shear reinforcement in the form of longitudinal reinforcement bars installed at mid-depth in the slab in order to increase its shear capacity.

5.3 *Conclusions*

A discrete beam model consisting of infinitely rigid segments and flexible hinges turns out to be a suitable aid for analysing the elasto-plastic response of reinforced concrete beams under impulsive loading. This has been achieved thanks to the fact that the equations obtained with such a model can be solved in a simple manner by making use of available systems for the integration of non-linear time-dependent equations – in our case emobidied in the DYNAMO system dynamics language.

In a simply-supported beam subjected to a uniformly distributed impulsive load the distribution of the bending moments and shear forces will differ considerably from that associated with a comparable static load. Presupposing that no shear failure will occur, plastic moments will be formed at some distance from mid-span. From here the plastic hinges will "move along" towards mid-span. In arriving at this response it has indeed been presumed that the impulsive loading is of sufficient magnitude to attain the plastic moment in the beam. If the load differs in this respect, a response as described in Section 5.1.3 will be obtained.

In the case of the fixed-end beam investigated here (representing a tunnel roof) the results are very different. The distribution of the moments is more closely similar in form to that obtained under static load, but the shear forces still differ from those in the static case, though this difference is less pronounced than for the simply-supported beam. Hence it follows that an analysis in which the tunnel roof is schematized to a single-mass spring system will determine the displacements and moments with sufficient accuracy. On the other hand, with this approach the magnitude and location of the maximum shear force may be incorrectly calculated!

If no stirrups are provided, a shear failure criterion will have to be introduced. This will greatly reduce the permissible load, and in most cases no plastic hinges will even be formed.

The type of tunnel roof investigated here will fail in shear if no special preventive arrangements are provided. Extra longitudinal reinforcement in the middle plane of the roof slab, or the use of steel-fibre-reinforced concrete, are means of increasing the shear strength of slabs without installing stirrup reinforcement. If stirrups are installed, they must be present over practically the full length of the tunnel roof slab.

6 Notation

A	cross-sectional area
A_s	reinforcing steel
A_{sv}	shear reinforcement
E	modulus of elasticity
$E_c\,(E_s)$	concrete (steel)
$E_{cd}\,(E_{sd})$	concrete dynamic (steel dynamic)
M	bending moment
M_{cr}	first flexural crack is formed
M_{sy}	reinforcing steel reaches yield point
M_p	plastic moment
M_u	ultimate (or failure) moment
V	shear force
$V_c\,(V_{cd})$	contribution of concrete zone (dynamic)
V_{sv}	contribution of vertical shear reinforcement
V_n	design shear force
V_u	total force at failure
V_j	at node j of mathematical model
C	spring stiffness
$\varkappa$	curvature
$\varkappa_{sy}$	reinforcing steel reaches yield point
$\varkappa_u$	ultimate curvature (curvature at failure)
EI	flexural stiffness
a	acceleration; length
b	width
d	effective depth
f	strength
f_c	concrete
f_{ct}	tensile strength
f_{ctd}	dynamic (impact) tensile strength
f_{cu}	compressive strength
f_{cc}	characteristic cube (compressive) strength
f_{cd}	dynamic compressive strength
f_s	reinforcing steel
f_{sy}	yield strength
f_{syd}	dynamic yield strength
h	depth of a section
l_p	plastic length
Φ	angular rotation
Φ_p	plastic rotation
Φ_{pu}	maximum plastic rotation if $V=0$
Φ_{pV}	maximum plastic rotation if $V\neq 0$

Φ_u	ultimate rotation (rotation at failure)
Φ_y	rotation at which reinforcement yields
w	displacement
$\dot{w} = v$	velocity
$w_{,xxxx}$	fourth partial derivative with respect to x
λ	length of segment
Δt	time step, approximately 1×10^{-5} s
α	proportionality factor
r	factor for determining rotational capacity
σ	stress
τ	shear stress
ε	strain

7 References

1. Rooduijn, E. J., Explosies in tunnels, (in Dutch). Graduation report, Delft Univ. of Techn., 1980.
2. Kani, G. N. J., How safe are our large reinforced Concrete Beams? Journal ACI, Proc. Vol. 64, no. 3, March 1967, pp. 128–141.
3. Walraven, J. C., Het afschuifdraagvermogen van grindbeton- en lichtbetonliggers zonder schuifwapening, (in Dutch). Betononderzoek 1976–1980, pp. 100–105.
4. Taylor, H. P. J., Shear strength of large beams. Proceedings of the ASCE, November 1972, pp. 2473–2490.
5. Swamy, Qureshi, Strength, Cracking and Deformation Similitude in Reinforced T-Beams under Bending and Shear. ACI-Journal, March 1971, pp. 187–195.
6. Reinhardt, H. W., Similitude of Brittle Fracture of Structural Concrete. IABSE Colloquium Delft 1981, pp. 175–184.
7. Hillerborg, A., Report to RILEM TC 50-FMC. Division of Building Materials Land Institute of Technology Feck., January 1981.
8. Zsutty, T. C., Beam shear strength prediction by analysis of existing data. ACI-Journal, Vol. 65, no. 11, Nov. 1968, pp. 941–951.
9. Zsutty, T. C., Discussion of the paper, ref. [8]. ACI-Journal, May 1969, pp. 435–438.
10. Leonhardt, F. und R. Walther, Schubversuche an Durchlaufträgern, (in German). DafStb., H 163, 1964.
11. Rodriguez, J. J. and A. C. Bianchini e.a., Shear strength of two-span continuous reinforced concrete beams. ACI-Journal, title no. 55–66, April 1959, pp. 1089–1140.
12. Rafla, K., Empirische Formeln zur Berechnung der Schubtragfähigkeit von Stahlbetonbalken, (in German). Teil I. Strasse, Brücke, Tunnel, December 1971, no. 12, pp. 311–320.
13. Walraven, J. C. and H. W. Reinhardt, Theory and experiments on the mechanical behaviour of cracks in plain and reinforced concrete subjected to shear loading. Heron, Vol. 26, no. 1A, 1981.
14. Walraven, J. C., Aggregate interlock: A theoretical and experimental analysis. Proefschrift, 8 October 1980.
15. Walraven, J. C., The behaviour of cracks in plain and reinforced concrete subjected to shear. IABSE Colloquium, Delft 1981, pp. 227–244.
16. Mattock, A. H. and N. M. Hawkins, Shear transfer in reinforced concrete recent research. PCI-Journal, March–April 1972, pp. 52–72.
17. Körmeling, H. A., A. J. Zielinski and H. W. Reinhardt, Experiments on concrete under single and repeated unaxial impact tensile loading. Stevin Report 5-80-3, Delft, 1980.
18. Zielinski, A. J., Fracture of concrete and mortar under unaxial impact tensile loading. Doctoral thesis, November 1982.

19. REINHARDT, H. W., Concrete under impact loading, Tensile strength and bond. Heron, Vol. 27, no. 3, 1982, pp. 31–35.
20. BAUMANN, T. und H. RÜSCH, Versuche zum Studium der Verdübelungswirkung der Biegezugbewehrung eines Stahlbetonbalkens, (in German). DAfStb. H. 210, 1970, pp. 46–83.
21. HAMADI, V. D., Behaviour in shear of beams with flexural cracks. Magazine of Concrete Research, Vol. 32, no. 10, March 1980, pp. 67–78.
22. MONNIER, TH. en P. W. VAN DE HAAR, Doorgaande balken van gewapend beton, (in Dutch). CUR-VB-Report 83, juni 1980.
23. BACHMANN, H., Influence of shear and bond on rotational capacity of reinforced concrete beams. International Association for Bridge and Structural Engineering, Publications 30-II, 1970.
24. SIVIERO, E., Rotation capacity of monodimensional members in structural concrete. CEB Bulletin d'Information, no. 105, Structural Hyperstatiques, 1976.
25. CORLEY, W. G., Rotation capacity of reinforced concrete beams. Journal of the Structural Division, Vol. 92, no. St 5, October 1966, pp. 121–146.
26. BURNS, H. and P. S. CHESTER, Plastic hinging in reinforced concrete. Journal of the Structural Division, Vol. 92, no. St 5, October 1966, pp. 45–78.
27. GIJSBERS, F. B. J., Onderzoek naar de rotatiecapaciteit van op buiging belaste liggers met een rechthoekige doorsnede van met FeB 400 HK gewapend grindbeton, (in Dutch). IBBC-TNO Report No. BI-74-6104.1.280, January 1974.
28. BEUKEL, A. VAN DEN, concept "Rotatiecapaciteit", (in Dutch). Verslag van een onderzoek opgesteld in samenwerking met CUR-VB-commissie A24 "Plastische scharnieren". IBBC-TNO Report No. BI-81-58/62.4.1120.
29. CUR-VB-report no. 108, "Plastische scharnieren", (in Dutch). Betonvereniging Zoetermeer, September 1982.
30. HAWKINS, N., Seattle report U.S. Navy. January 1982.
31. NELISSEN, L. J. M., Twee-assig onderzoek van grindbeton, (in Dutch). Heron, Vol. 18, 1972.
32. HJORTH, O., Ein Beitrag zur Frage der Festigkeiten und des Verbundverhaltens von Stahl und Beton bei hohen Beanspruchungsgeschwindigkeiten, (in German). Dissertation 1976, Technische Universität Braunschweig.
33. KVIRIKADZE, O. P., Determination of the ultimate strength and modulus of deformation of concrete at different rates of loading. Int. Symposium on testing in situ of concrete structures, Budapest, 1977, pp. 109–117.
34. MAINSTONE, R. J., Properties of materials at high rates of straining or loading. Matériaux et constructions, Vol. 8, no. 44.
35. VOS, E. and H. W. REINHARDT, Bond resistance of deformed bars, plain bars and strands under impact loading. SR-35, 1980, Delft Univ. of Techn.
36. Concrete structures under impact and impulsive loading. BAM, proceedings, Berlin (West), June 2–4, 1982, pp. 135–156.
37. THOMPSON, K. J. and R. PARK, Seismic response of partially prestressed concrete. Journal of the Structural Division, Vol. 106, no. ST 8, ASCE, Aug. 1980, pp. 1755–1774.
38. PARK, R. and K. J. THOMPSON, Cyclic load tests on prestressed and partially prestressed concrete beam-column joints. Journal of the Prestressed Concrete Institute, Vol. 22, no. 5, Sept.-Oct. 1977.
39. HUMAR, J., Seismic response of reinforced concrete frames. Journal of the Structural Division, Vol. 107, no. ST 7, ASCE, July 1981.
40. MONIER, TH., The moment-curvature relation of reinforced concrete. Heron, Vol. 17, no. 2, 1970.
41. POPOV, E. P., Seismic behaviour of Structural Subassemblages. Journal of the Structural Division, Vol. 100, no. ST 7, ASCE, July 1980, pp. 1460–1774.
42. BRUGGELING, A. S. G., Het gedrag van betonconstructies, (in Dutch). Part B, XC-pp. 23.
43. BLAAUWENDRAAD, J., Methoden en mogelijkheden voor het electronisch berekenen van op buiging belaste platen, (in Dutch). De Ingenieur TWO 3, 7 February 1969.
44. PUGH, A. L., Dynamo User's Manual. Fifth edition, The MIT Press, Cambridge, Massachusetts, and London, England.

45. System Dynamics Manual. Delft Univ. of Techn., Dept. of Civil Eng., Sept. 1976.
46. BLAAUWENDRAAD, J. en A. W. M. KOK, Elementenmethode 1 voor constructeurs, (in Dutch). Agon Elsevier Amsterdam/Brussels 1973, pp. 173–178.
47. BLAAUWENDRAAD, J. en A. W. M. KOK, Elementenmethode; Dynamica Moduul, (in Dutch). Stichting Postdoctoraal Onderwijs in de Civiele Techniek, Delft Univ. of Techn., May 1982.
48. VEEN, C. VAN DER, Explosies in Tunnels, (in Dutch). Graduation report TH-Delft, September 1982.